MEGANOMALY: EXTENDING UNSUPERVISED ANOMALY DETECTION TO HUNDREDS OF CATEGORIES

Anonymous authors
Paper under double-blind review

ABSTRACT

Recent multi-class unsupervised anomaly detection (MUAD) methods have nearly closed the gap with their single-class counterparts on small-scale benchmarks, yet suffer severe degradation when extended to hundreds of categories. This degradation is commonly attributed to over-generalization, where the reconstruction network learns to restore unseen anomalous patterns. In this work, we show that this explanation is incomplete. Through controlled scaling experiments, we identify **capacity saturation** as a critical overlooked factor: as the number of categories grows, diverse normal patterns compete and interfere within the decoder's finite weights, causing normal reconstruction to saturate while anomaly reconstruction continues to improve. Guided by this insight, we present **Meganomaly**, a framework for large-scale MUAD based on a simple design principle: expanding decoder's capacity. Specifically, ShareMLP composes image-adaptive MLPs from a dynamic weight pool shared across decoder layers, substantially increasing capacity and reducing inter-category interference at little additional computational cost. To prevent anomalies from exploiting this expanded capacity, the Prior-Preserving Tight Bottleneck (PTB) aggressively compresses content information while preserving spatial and semantic priors that reconstruction relies on. Extensive experiments on seven datasets show that Meganomaly establishes state-of-the-art on large-scale benchmarks, improving I-AUROC by +5.5% on Real-IAD Variety (94.6%, 160 classes) and +7.1% on ADNet (89.1%, 380 classes).

1 INTRODUCTION

Unsupervised anomaly detection (UAD) aims to learn normal patterns from normal-only data and identify anomalous deviations at test time, serving as a fundamental task in computer vision. Its applications span diverse domains including industrial inspection (Bergmann et al., 2019; Wang et al., 2024), medical diagnosis (Xiang et al., 2024; Guo et al., 2023a), and surveillance systems (Mabrouk & Zagrouba, 2018; Yao et al., 2022). Since anomalies are inherently scarce and unpredictable, models must learn to represent normal patterns from normal-only data and flag deviations during inference. The reconstruction-based paradigm (Akcay et al., 2018; Deng & Li, 2022), rooted in the epistemic behavior (Kendall & Gal, 2017) of neural networks, has become a mainstream solution: a model trained exclusively on normal data is expected to accurately reconstruct normal patterns while failing on anomalous ones.

Early UAD methods follow a *one-class-one-model* paradigm (Roth et al., 2022; Deng & Li, 2022), training a separate model for each object category. Although effective in controlled settings, the storage overhead and maintenance burden of managing hundreds of individual models become prohibitive in large-scale deployments. This has motivated the shift toward multi-class UAD (MUAD), where a single model handles all categories simultaneously (You et al., 2022). However, this unification typically comes with a substantial performance drop relative to single-class training. Previous works (You et al., 2022; Guo et al., 2025b) identified the central challenge of MUAD as *over-generalization* (also termed *identity mapping*): when trained on diverse categories, the reconstruction decoder may acquire sufficient generalization to restore even unseen anomalous patterns, thereby undermining anomaly detection based on reconstruction error.

Reviewers: please read the Reviewer Guidelines (iclr.cc/Conferences/2027/ReviewerGuidelines) and the AI Policy for Reviewers (iclr.cc/Conferences/2027/AIPolicyForReviewers). If you used AI to expand, edit, or polish your review, please provide the input text to the LLM. Better still, consider skipping the LLM and submitting your original text: we, and the authors, are much more interested in your unedited thoughts than in what an LLM has to say. AI-assisted or not, you are putting your name and reputation behind your review: LLM-generated falsehoods, hallucinations or misrepresentations are subject to disciplinary action, which may include desk-rejecting all papers you have authored.

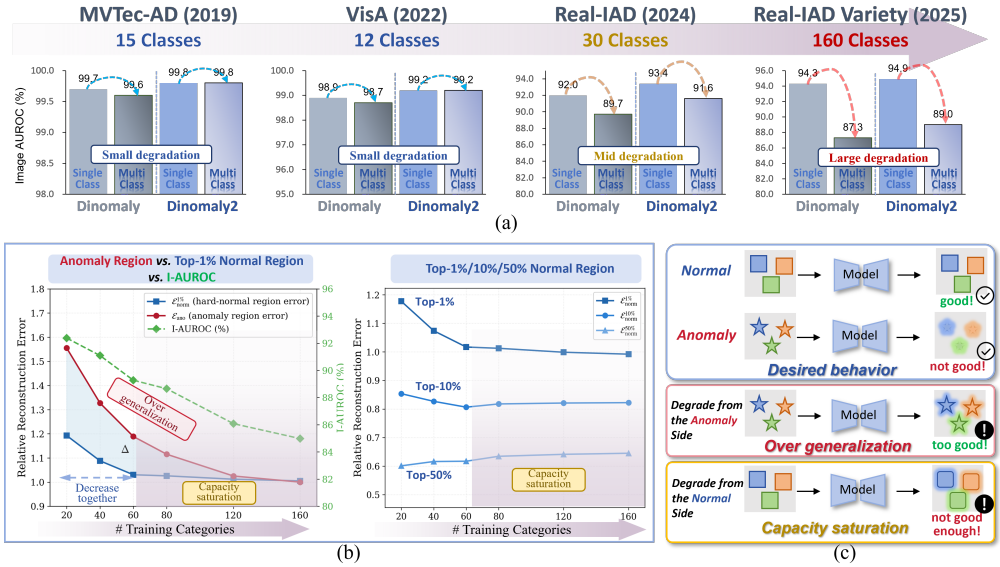


Figure 1: **Motivation and diagnosis of large-category MUAD degradation.** (a) The performance gap between single-class and multi-class models widens dramatically as the number of categories increases. (b) Scaling behavior of the Dinomaly2 baseline on Real-IAD Variety (Zhu et al., 2026). Models are trained on 20–160 categories until convergence and evaluated on the fixed first 20-category test set. As category diversity increases, the anomaly region error consistently decreases. The top-1% normal region error (hard-normal), together with top-10%/50% normal errors, begins to saturate or even increase. (c) Conceptual illustration of the two coupled failure modes: over-generalization shrinks the reconstruction gap from the anomaly side, whereas capacity saturation shrinks it from the normal side.

To address the issue of over-generalization, a series of techniques have been proposed, including neighbor-masked attention (You et al., 2022), synthetic anomalies (Zhao, 2023), vector quantization (Lu et al., 2023), diffusion models (Yin et al., 2023; He et al., 2024b), and state space models (He et al., 2024a). More recently, several methods (Guo et al., 2025b;a) have reported that the gap between multi-class and single-class UAD has been largely eliminated, achieving near-perfect image-level detection on MVTec-AD (Bergmann et al., 2019) (99.8% I-AUROC) and VisA (Zou et al., 2022) (99.2%).

However, these advances are largely confined to a *small-scale comfort zone*. The emergence of large-scale multi-class benchmarks (*e.g.*, Real-IAD Variety (Zhu et al., 2026) with 160 categories, ADNet (Ling et al., 2025) with 380 categories) reveals a harsh reality: even state-of-the-art (SOTA) MUAD methods suffer severe performance degradation when the number of categories scales to hundreds. As shown in Fig. 1(a), Dinomaly2 (Guo et al., 2025a), achieves 94.9% image-level AUROC on Real-IAD-Variety when separate models are trained per class, yet drops to 89.0% under a unified multi-class model. This stands in stark contrast to the near-perfect scores on MVTec-AD and VisA.

Why do existing methods fail at scale? We uncover **capacity saturation** of normal reconstruction as a previously overlooked factor through controlled experiments on Real-IAD Variety, training on 20 to 160 categories and evaluating on a fixed subset of 20 classes (Fig. 1(b)). As the number of categories grows, the decoder's capacity is increasingly shared among diverse normal patterns, causing normal reconstruction quality to plateau or even degrade. Meanwhile, anomaly reconstruction continues to improve as the decoder encounters richer training distributions. In other words, *the performance degradation in large-scale MUAD is not merely because anomalies are reconstructed too well, but also because normal patterns are not reconstructed well enough* (Fig. 1(c)). This insight identifies an additional requirement for scaling MUAD: beyond preventing over-generalization, scaling MUAD requires expanding the model's capacity.

Guided by this insight, we present **Meganomaly**, a framework for scaling MUAD to hundreds of categories. We translate the diagnosis into a simple design principle: expanding the decoder's effective capacity without substantially increasing computational cost or architectural complexity. To

begin with, ShareMLP implements a dynamic weight mechanism where all decoder layers draw from a common pool of weight bases and compose layer-specific, image-adaptive soft MLPs via lightweight routing. By sharing weight bases across layers, the space of realizable decoder functions grows combinatorially at little extra computation. Different categories can route to distinct weight combinations, forming implicit class-specific pathways that relieve inter-category interference. To prevent anomalous patterns from exploiting this increased capacity, Prior-Preserving Tight Bottleneck (PTB) aggressively compresses the bottleneck's intermediate dimension to restrict excessive information flow, while selectively preserving positional and semantic priors that reconstruction relies on but over-generalization can hardly exploit.

Extensive experiments demonstrate that Meganomaly establishes new SOTA performance on challenging UAD benchmarks including Real-IAD(Wang et al., 2024) (30 classes, I-AUROC=93.1%), MANTA (Fan et al., 2025a) (38 classes, 94.3%), Real-IAD Variety (Zhu et al., 2026) (160 classes, 94.6%), and ADNet (Ling et al., 2025) (380 classes, 89.1%).

2 Related Work

Unsupervised Anomaly Detection. Existing image UAD methods can be broadly grouped into several paradigms. Reconstruction or distillation methods train a decoder or student network to reconstruct features from a pre-trained encoder, using reconstruction discrepancies as anomaly scores (Deng & Li, 2022; Salehi et al., 2021). Synthetic-anomaly methods generate artificial defects and formulate anomaly detection as supervised discrimination or segmentation (Li et al., 2021; Zavrtanik et al., 2021), but their performance depends on the design of synthetic defects. Memory-based methods store normal features and detect anomalies by nearest-neighbor matching (Defard et al., 2021; Roth et al., 2022), but their memory and computation costs grow with the training set size. Among these, reconstruction-based methods are particularly attractive for multi-class settings due to their simplicity and scalability.

Multi-Class UAD. Early UAD methods typically follow a one-class-one-model paradigm. Multi-class UAD instead uses a unified model for multiple categories (You et al., 2022). A central challenge in this setting is over-generalization, also known as identity mapping, where the reconstruction model restores anomalous regions too well and weakens anomaly-normal separability. Existing works address this issue using masked attention, synthetic anomalies, contrastive learning, diffusion models, state space models, or improved reconstruction objectives (You et al., 2022; Zhao, 2023; Gao, 2024a; Guo et al., 2023b; He et al., 2024a; Meng et al., 2024; Fan et al., 2025b; Wang et al., 2025b; Guo et al., 2025b). While recent methods report near-elimination of the gap between multi-class and single-class UAD on small benchmarks, their performance still degrades substantially when extended to hundreds of categories.

Expanding Network Capacity. Increasing model capacity is a common strategy for handling diverse data distributions. Mixture-of-Experts (MoE) methods expand capacity through conditional computation, and have been widely studied in language and vision models (Shazeer et al., 2017; Fedus et al., 2022). However, standard MoE typically relies on per-token routing, which may be undesirable for UAD because it could allow anomalous tokens to exploit experts specialized for other categories. Another line of work uses dynamic weights and convolutions, where network parameters are composed conditioned on the input (Yang et al., 2019; Chen et al., 2020; Li et al., 2022; Li & Yao, 2024). In this work, we simplify and adapt these ideas to boost large-scale UAD by increasing model capacity. Due to space limitations, we provide an extended discussion of related work in Appendix A.1.

3 Method

Meganomaly starts from state-of-the-art reconstruction-based UAD frameworks, *e.g.*, ViTAD, Dinomaly (see Appendix A.2 for preliminaries). We first show that this framework suffers from capacity saturation as the number of categories grows (Sec. 3.1). This motivates a capacity-first design: ShareMLP expands the decoder's effective capacity (Sec. 3.2), while PTB prevents the added capacity from facilitating anomaly reconstruction (Sec. 3.3).

3.1 RETHINKING THE CRUX OF LARGE-SCALE MUAD

Prior works (You et al., 2022; Guo et al., 2025b) attribute the performance degradation of MUAD to *over-generalization*: as category diversity increases, the decoder generalizes its reconstruction ability to unseen anomalous patterns. Here, we show that this explanation is incomplete when the number of categories scales to hundreds.

To isolate the effect of category count, we conduct a controlled diagnostic experiment on Real-IAD Variety (Zhu et al., 2026), as shown in Fig. 1(b). We train Dinomaly2-S (Guo et al., 2025a) on $C \in \{20, 40, 60, 80, 120, 160\}$ categories and evaluate all models on the same fixed first 20-category test set. This protocol keeps the evaluation set fixed as training-category diversity increases. We measure the reconstruction error inside annotated anomalous regions, denoted as $\mathcal{E}_{\text{ano}}$, and the mean reconstruction error over the top-1/10/50% normal regions, denoted as $\mathcal{E}_{\text{norm}}^{1/10/50\%}$. Reported errors are normalized by the anomaly-region reconstruction error at $C{=}160$.

Key Findings. The results in Fig. 1(b) reveal two distinct trends:

(1) Anomaly reconstruction keeps improving. Anomalous-region errors $\mathcal{E}_{\text{ano}}$ consistently decrease as more categories are included for training. This is consistent with the **over-generalization** hypothesis: exposure to more diverse normal patterns enables the decoder to increasingly generalize to anomalous patterns.
(2) Normal reconstruction saturates. Normal-region errors $\mathcal{E}_{\text{norm}}$ stop improving after the early stage. As category diversity grows, $\mathcal{E}_{\text{norm}}^{1\%}$ starts to plateau, while broader regions $\mathcal{E}_{\text{norm}}^{10\%}$ and $\mathcal{E}_{\text{norm}}^{50\%}$ even increase. This reflects **capacity saturation**: diverse normal patterns compete and interfere within the decoder's finite, shared weights.

These findings show that large-scale MUAD degradation is caused by two coupled failure modes. Over-generalization shrinks the reconstruction gap from the anomaly side, whereas capacity saturation shrinks it from the normal side.

Implications for Method Design. These findings reveal that the conventional focus on suppressing over-generalization addresses only one side of the problem. We therefore aim to expand the decoder's effective capacity to accommodate normal patterns from hundreds of categories. Because unconstrained expansion could also improve anomaly reconstruction, the added capacity must be paired with appropriate information control. Meganomaly (Fig. 2) realizes this dual-strategy through ShareMLP and PTB.

3.2 SHAREMLP: EXPANDING DECODER CAPACITY

A straightforward remedy to capacity saturation is to increase the decoder width or depth, but this incurs proportional computation overhead. Effective capacity depends not only on the number of parameters but also on how they are allocated; we improve both while keeping inference cost nearly unchanged.

From Standard MLP to DynaMLP. In a standard Transformer decoder, each layer's feed-forward network (FFN) applies fixed linear transformations (Fig.3(a)):

$$\text{FFN}(\mathbf{h}) = \mathbf{W}_2\,\sigma(\mathbf{W}_1\mathbf{h} + \mathbf{b}_1) + \mathbf{b}_2, \tag{1}$$

where $\mathbf{W}_1 \in \mathbb{R}^{4d\times d}$, $\mathbf{W}_2 \in \mathbb{R}^{d\times 4d}$, and σ is the activation function (GELU). These weights are shared by all inputs regardless of category. Statically widening the FFN adds capacity, but all categories still compete within the same weights; assigning each category a separate FFN removes this interference, but scales parameters linearly with the number of categories.

A natural first step is to make the weights input-dependent. Inspired by dynamic convolutions (Yang et al., 2019; Chen et al., 2020), we introduce DynaMLP (Fig.3(b)). We maintain K sets of weight bases per layer and compose them via routing weights derived from the `CLS` token:

$$\mathbf{W}_1^{(l)} = \sum_{k=1}^{K} \alpha_k^{(l)} \mathbf{W}_{1,k}^{(l)}, \quad \boldsymbol{\alpha}^{(l)} = \text{Softmax}\big(\phi^{(l)}(\mathbf{f}^{cls})\big), \quad \alpha^{(l)} \in \mathbb{R}^K, \tag{2}$$

where $\phi^{(l)}$ is a lightweight router (a single linear layer) at decoder layer l, and $\mathbf{f}^{cls}$ is the `CLS` token of this layer's input. The same routing applies to $\mathbf{W}_2^{(l)}$. Crucially, routing is performed at the

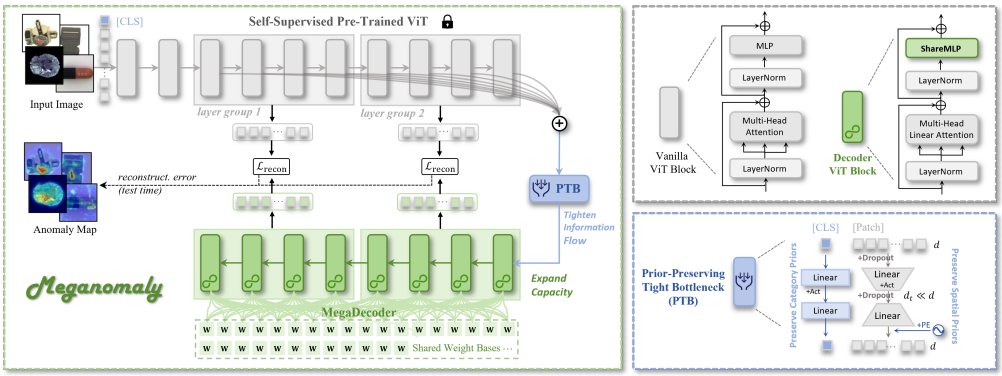


Figure 2: **Overview of the Meganomaly framework.** A pre-trained ViT encoder extracts multi-layer features, which are aggregated and passed through the **Prior-Preserving Tight Bottleneck** (PTB) into the MegaDecoder, where the **ShareMLP** replaces the standard MLP. The reconstruction error between encoder and decoder features serves as the anomaly score.

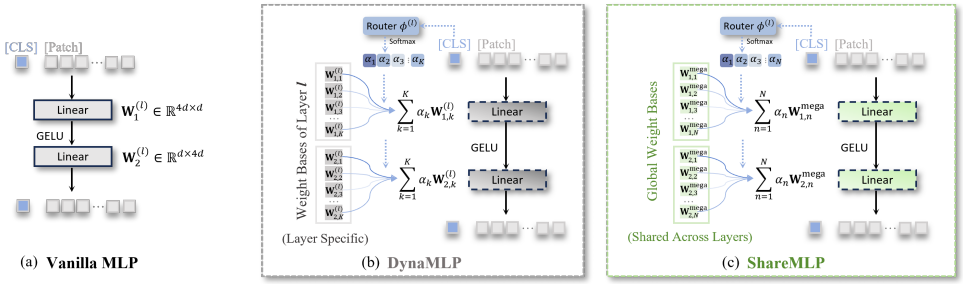


Figure 3: **ShareMLP.** (a) A standard MLP uses fixed weights. (b): DynaMLP maintains K per-layer weight bases and composes them via `[CLS]`-conditioned routing. (c) ShareMLP shares a global pool of N weight bases across all decoder layers, giving each layer access to the full pool through layer-specific routers.

image level rather than per token: all spatial tokens in the same image share the same composed weights. This avoids the pitfall of standard sparse MoE (Shazeer et al., 2017), where per-token routing could dispatch anomalous patches to the experts that reconstruct them best. Meanwhile, input-conditioned routing allows different categories to use different weight combinations, which can mitigate interference among their reconstruction demands. Note that the `CLS` token in ViTs encodes image-level global context through self-attention, and does not require any category label supervision.

Cross-Layer Weight Sharing. DynaMLP increases per-layer capacity, but its K weight bases are private to each layer, limiting the total number of bases under a fixed parameter budget. We observe that decoder layers across different depths perform related reconstruction tasks within the same feature space ($d \to 4d \to d$), suggesting that their weight bases can be productively shared.

This motivates ShareMLP (Fig.3(c)). Inspired by parameter sharing (Zhong et al., 2025; Savarese & Maire, 2019), we introduce a single shared pool of N weight bases that all L_d decoder layers draw from:

$$\mathbf{W}_1^{(l)} = \sum_{n=1}^{N} \alpha_n^{(l)} \mathbf{W}_{1,n}^{\text{mega}}, \quad \alpha^{(l)} \in \mathbb{R}^N. \tag{3}$$

Each decoder layer retains its own router $\phi^{(l)}$ to produce layer-specific routing weights, but all routers select from the same pool $\{\mathbf{W}_{1,n}^{\text{mega}}\}_{n=1}^{N}$ (and analogously for $\mathbf{W}_2$). By default, we set N=64.

Here, each layer's effective capacity grows from K (per-layer) to N (shared) bases without increasing the total parameter count. Since each of the L_d layers independently routes over the shared pool, the decoder can realize diverse layer-wise weight combinations, yielding an effective function diversity exceeding the linear growth in parameters. In practice, different categories naturally

self-organize into distinct routing patterns, forming implicit class-specific reconstruction pathways without explicit supervision.

3.3 Prior-Preserving Tight Bottleneck

The expanded decoder capacity is intended to improve normal reconstruction, but without proper information control it could also make anomalies easier to reconstruct. We therefore introduce the Prior-Preserving Tight Bottleneck (PTB; Fig. 2, lower right) as a safeguard: it tightly restricts the content information flowing into the decoder while preserving two types of priors that are critical for reconstruction quality.

Tight Compression. Recall from Sec. A.2 that the standard noisy bottleneck $\mathcal{B}$ uses an MLP with Dropout at the standard FFN expansion ratio ($d \to 4d \to d$). We argue that this generous intermediate dimension allows excessive content information to survive the stochastic masking. We replace it with a much narrower MLP:

$$\mathbf{z}^{patch} = \mathbf{W}_2' \,\text{Dropout}\big(\sigma(\mathbf{W}_1' \mathbf{h}^{patch})\big), \quad \mathbf{W}_1' \in \mathbb{R}^{d_t \times d},\ \mathbf{W}_2' \in \mathbb{R}^{d \times d_t}, \tag{4}$$

where $d_t \ll d$. This aggressive compression forces the decoder to reconstruct from minimal information. However, not all information should be discarded equally. We identify two types of priors that are essential for reconstruction and explicitly preserve them.

Preserving Spatial Priors. Unlike CNNs, ViTs do not encode spatial locality in their architecture, *i.e.*, positional information is carried entirely through positional embeddings and propagated via attention. The narrow bottleneck has limited capacity to jointly encode both semantic content and positional information. Therefore, we compensate by adding a positional embedding $\mathbf{PE} \in \mathbb{R}^{N \times d}$ to the bottleneck output: $\mathbf{z}' = \mathbf{z} + \mathbf{PE}$. This provides an explicit spatial prior, restoring the decoder's ability to leverage positional context without reintroducing the detailed content information.

Preserving Semantic Priors. The `CLS` token serves a dual role: it encodes image-level semantics and drives routing in ShareMLP. Passing it through the same noisy pathway would corrupt the routing signal and destabilize dynamic weight composition across all decoder layers. We therefore process the `CLS` token through a separate MLP *without* Dropout, as illustrated in Fig. 2.

4 Experiments

4.1 Experimental Setup

Datasets. We evaluate Meganomaly on seven benchmarks spanning three scales of category diversity. *Large-scale:* **Real-IAD Variety** (Zhu et al., 2026) is the largest multi-view industrial anomaly detection benchmark, containing 160 object categories from 28 industries, each captured from 5 camera views. **ADNet** (Ling et al., 2025) is a multi-domain benchmark aggregating 380 categories from public datasets across five domains (Electronics, Industry, Agrifood, Infrastructure, and Medical). *Mid-scale:* **Real-IAD** (Wang et al., 2024) is a widely used multi-view dataset containing 30 industrial product categories. **MANTA** (Fan et al., 2025a) is a multi-view dataset for tiny objects (*e.g.*, various seeds and beans) comprising 38 categories. We use the official MANTA-Tiny split. *Small-scale:* **MVTec-AD** (Bergmann et al., 2019) is the most established UAD benchmark with 15 categories. **VisA** (Zou et al., 2022) contains 12 categories focusing on complex patterns. **Uni-Medical** (Zhang et al., 2024) is a medical UAD benchmark covering three imaging modalities, with substantially larger intra-class variation than industrial datasets.

Implementation. Dinomaly2 (Guo et al., 2025a) is used as the baseline framework by default. Unless otherwise specified, we use DINOv2R-B (Darcet et al., 2024) as the frozen encoder and reconstruct features from its middle 8 layers. MegaDecoder contains 8 layers with a shared ShareMLP pool of N=64 bases, and PTB uses d_t=32 with a Dropout rate of 0.4 by default. Models are trained with StableAdamW (Wortsman et al., 2023) using a batch size of 16 for 100K iterations by default, and 40K iterations on small-scale datasets. Further details are provided in Appendix A.2.

Metrics. Image-level (I-) anomaly detection is measured by AUROC, AP, and F_1 score at the optimal threshold (F_1-max). Pixel-level (P-) anomaly localization is measured by AUROC, AP, F_1-max, and AUPRO. For multi-view datasets, we additionally report object-level metrics (O-). All results are averaged across categories within each dataset.

Table 1: Results on large-scale benchmarks under the multi-class UAD setting. Best results are in **bold** and second best are underlined.

Method	Image-level			Object-level			Pixel-level			
	AUROC	AP	F_1-max	AUROC	AP	F_1-max	AUROC	AP	F_1-max	AUPRO
Real-IAD Variety (Zhu et al., 2026), 160 categories										
RD4AD (Deng & Li, 2022)	72.0	93.6	93.5	76.7	95.6	95.1	88.8	22.3	28.1	68.8
SimpleNet (Liu et al., 2023)	62.1	91.4	93.1	70.3	94.6	94.5	78.1	9.7	14.3	42.1
UniAD (You et al., 2022)	67.1	92.3	93.3	67.9	93.7	94.5	87.0	17.9	23.9	62.1
ViTAD (Zhang et al., 2025b)	78.3	95.4	93.7	83.6	97.2	95.6	90.9	31.9	36.3	70.3
MambaAD (He et al., 2024a)	79.0	95.6	93.7	85.0	97.4	95.6	90.2	30.9	35.5	70.6
Dinomaly (Guo et al., 2025b)	87.3	97.5	94.8	92.5	98.9	97.1	93.5	44.0	47.0	79.5
INP-Former (Luo et al., 2025)	87.5	97.6	94.7	91.8	98.8	96.7	93.6	46.4	47.9	78.6
EILA (Liu et al., 2026)	87.1	97.5	94.7	91.3	98.6	96.8	93.8	44.5	46.8	78.6
Dinomaly-MoE (Meng et al., 2024)	88.8	97.8	95.2	93.4	99.0	97.4	94.3	46.8	49.1	81.6
Dinomaly2 (Guo et al., 2025a)	89.0	97.9	95.1	94.2	99.1	97.5	94.0	50.5	51.5	81.8
Meganomaly (Ours)	**94.6**	**98.9**	**96.6**	**97.8**	**99.7**	**98.7**	**95.8**	**53.9**	**54.5**	**85.4**
ADNet (Ling et al., 2025), 380 categories										
RD4AD (Deng & Li, 2022)	66.9	83.2	86.4	–	–	–	87.4	15.7	21.2	69.3
SimpleNet (Liu et al., 2023)	52.7	75.9	84.0	–	–	–	65.0	3.9	7.5	32.8
UniAD (You et al., 2022)	63.4	81.5	85.8	–	–	–	86.7	11.8	17.4	66.3
ViTAD (Zhang et al., 2025b)	72.4	86.3	87.9	–	–	–	88.1	19.6	24.4	68.2
MambaAD (He et al., 2024a)	72.7	87.0	87.8	–	–	–	88.8	20.7	25.8	71.3
Dinomaly (Guo et al., 2025b)	78.1	89.7	89.8	–	–	–	90.1	22.3	28.1	73.3
INP-Former (Luo et al., 2025)	77.2	89.4	89.6	–	–	–	90.5	23.3	28.9	73.8
EILA (Liu et al., 2026)	78.4	89.9	89.9	–	–	–	91.2	25.2	30.2	74.7
Dinomaly-MoE (Meng et al., 2024)	78.9	89.8	90.0	–	–	–	90.8	23.2	29.1	74.2
Dinomaly2 (Guo et al., 2025a)	82.0	91.4	91.0	–	–	–	93.1	32.9	37.2	81.4
Meganomaly (Ours)	**89.1**	**94.8**	**93.2**	–	–	–	**94.9**	**39.7**	**43.9**	**85.7**

4.2 Main Results on Large, Mid, and Small-Scale Benchmarks

Here, we present comprehensive results on seven MUAD benchmarks. On the two largest benchmarks (Tables 1), Meganomaly obtains substantial gains. It achieves 94.6% I-AUROC on Real-IAD Variety (Zhu et al., 2026) (160 categories), and 89.1% on ADNet (Ling et al., 2025) (380 categories), improving over Dinomaly2 by +5.5% and +7.1%, respectively. The improvements are consistent across evaluation metrics, including +3.5% O-AUROC and +3.6% AUPRO on Real-IAD Variety. On mid-scale benchmarks (Tables 2), Meganomaly also consistently improves over prior methods, reaching 93.1% I-AUROC on Real-IAD (Wang et al., 2024) and 94.3% on MANTA (Fan et al., 2025a), outperforming Dinomaly2 by +1.5% and +2.1%. On small-scale benchmarks (Tables A1), MVTec-AD (Bergmann et al., 2019) and VisA (Zou et al., 2022), it performs on par with Dinomaly2, where performance is already near saturation. On Uni-Medical (Zhang et al., 2024), Meganomaly also brings clear improvements, showing its effectiveness beyond industrial inspection. Overall, the gains increase with data diversity, supporting our diagnosis that capacity saturation is most critical in large-category MUAD.

4.3 Ablation Study

All ablation experiments are conducted on Real-IAD Variety (Zhu et al., 2026) with 160 classes. Meganomaly-S with DINOv2R-S (ViT-S) is used by default for efficiency.

Component Ablation. Table 3 ablates the two proposed components, starting from the Dinomaly2-S baseline (#1). Replacing the static MLP with DynaMLP (#2) improves I-AUROC from 86.34% to 91.66%, and ShareMLP (#3) further improves it to 92.00%, showing that image-adaptive and cross-layer shared weights effectively alleviate capacity saturation. Replacing NB with PTB (#4) improves the baseline to 90.10%, indicating that tighter prior-preserving information control independently benefits large-category MUAD. Combining ShareMLP with PTB (#6) achieves the best I-AUROC of 93.99%, demonstrating that expanded decoder capacity and tightened information flow are complementary. Table A3 further shows that ShareMLP achieves substantial gains even with simple Linear or MLP bottlenecks, without relying on the dedicated information constraints.

FFN Design. All evaluated capacity-expansion strategies improve over the static MLP baseline (Table 4), consistent with our capacity-saturation diagnosis. Statically widening the MLP yields diminishing returns, since the added parameters remain shared by all categories and interference persists. Sparse MoE (Shazeer et al., 2017) offers a better parameter-efficiency trade off, but per-token routing limits its effectiveness. DY-Conv (Chen et al., 2020), CondConv (Yang et al., 2019), and KW-Conv (Li & Yao, 2024) improve performance using complex dynamic convolution mech-

Table 2: Results on mid-scale benchmarks under the multi-class UAD setting.

Method	Image-level			Object-level			Pixel-level			
	AUROC	AP	F_1-max	AUROC	AP	F_1-max	AUROC	AP	F_1-max	AUPRO
Real-IAD (Wang et al., 2024), 30 categories										
RD4AD (Deng & Li, 2022)	83.0	79.6	74.4	85.7	92.4	87.7	97.3	25.8	33.5	90.4
SimpleNet (Liu et al., 2023)	82.6	79.2	74.1	61.2	77.9	82.1	76.3	3.4	6.9	42.5
UniAD (You et al., 2022)	83.0	83.4	74.6	87.3	93.1	88.9	97.4	23.7	31.4	87.3
ViTAD (Zhang et al., 2025b)	82.8	80.0	73.7	88.8	94.3	89.3	97.1	23.9	31.8	84.3
MambaAD (He et al., 2024a)	86.9	85.2	77.5	90.0	95.2	89.9	98.5	32.5	38.4	91.2
Dinomaly (Guo et al., 2025b)	89.7	87.1	80.5	92.8	96.3	92.3	98.9	43.8	47.8	94.6
INP-Former (Luo et al., 2025)	90.1	88.2	81.2	92.6	96.3	92.2	98.8	46.9	49.6	94.1
EILA (Liu et al., 2026)	90.4	88.1	81.5	92.9	96.6	91.9	98.9	43.3	47.4	94.3
Dinomaly2 (Guo et al., 2025a)	91.6	89.8	82.6	94.3	97.2	92.9	99.2	47.8	51.1	96.0
Meganomaly (Ours)	**93.1**	**90.9**	**84.8**	**96.4**	**98.3**	**95.0**	**99.4**	**48.3**	**51.5**	**97.0**
MANTA (Fan et al., 2025a), 38 categories										
RD4AD (Deng & Li, 2022)	81.2	63.7	64.0	78.7	68.8	69.7	91.5	28.1	33.1	77.6
SimpleNet (Liu et al., 2023)	72.8	53.8	52.8	75.5	66.7	63.4	83.4	13.5	18.7	53.8
UniAD (You et al., 2022)	84.7	69.7	68.1	82.4	71.5	71.7	90.4	24.6	31.2	78.9
ViTAD (Zhang et al., 2025b)	88.8	77.5	73.0	89.5	83.7	79.3	94.9	40.5	44.2	81.9
MambaAD (He et al., 2024a)	86.9	75.5	71.4	87.8	81.8	77.3	93.9	37.2	41.7	81.0
Dinomaly (Guo et al., 2025b)	91.1	82.1	77.0	92.1	88.1	82.7	95.1	44.8	48.5	84.1
INP-Former (Luo et al., 2025)	91.1	81.9	76.6	92.5	88.3	83.1	95.1	45.8	49.0	85.0
EILA (Liu et al., 2026)	91.8	82.9	78.2	92.5	88.5	83.1	95.6	47.1	49.9	85.0
Dinomaly2 (Guo et al., 2025a)	92.2	83.7	79.0	93.2	89.5	84.2	96.1	**51.6**	53.1	88.3
Meganomaly (Ours)	**94.3**	**87.7**	**83.4**	**95.5**	**92.9**	**88.3**	**96.2**	49.8	**53.2**	**90.1**

Table 3: Component ablation on Real-IAD Variety (160 classes). NB: Noisy Bottleneck; PTB: Prior-Preserving Tight Bottleneck. We start from #1: Dinomaly2-S.

#	Decoder FFN			Bottleneck		Image-level			Object-level			Pixel-level			
	MLP	DynaMLP	ShareMLP	NB	PTB	AUROC	AP	F_1-max	AUROC	AP	F_1-max	AUROC	AP	F_1-max	AUPRO
1	✓			✓		86.34	97.37	94.49	92.78	98.93	97.05	93.02	46.27	48.11	79.21
2		✓		✓		91.66	98.40	95.68	95.91	99.38	98.05	94.98	53.79	53.86	83.86
3			✓	✓		**92.00**	**98.48**	**95.74**	**96.26**	**99.44**	**98.16**	**95.12**	**54.41**	**54.37**	**84.23**
4	✓				✓	90.10	98.14	95.10	95.38	99.31	97.74	94.02	51.23	52.17	82.07
5		✓			✓	93.48	98.76	96.19	97.08	99.57	98.45	95.40	**53.77**	54.13	**84.81**
6			✓		✓	**93.99**	**98.82**	**96.35**	**97.34**	**99.60**	**98.57**	**95.46**	53.37	**54.25**	84.59

anisms. But they yield smaller gains than DynaMLP and ShareMLP, which can be more suitable in ViT-based UAD framework. Cross-layer sharing in ShareMLP make further improvements. Appendix Table A4 examines additional design choices for ShareMLP.

Bottleneck Design. Table 5 ablates PTB. Directly compressing the bottleneck from $4d$ to 32 hurts performance, as useful spatial information is lost. Adding positional embeddings recovers this loss, and using a separate noise-free `CLS` pathway yields the highest I-AUC and O-AUC. Overly narrow bottlenecks hurt localization, while larger d_t can improve localization at the expense of image-level detection. We choose d_t=32 to prioritize image-level defect screening in industrial UAD. Table A5 further shows that simply increasing Dropout in NB to restrict information is ineffective, whereas PTB remains stable across dropout rates.

Number of Weight Bases. Table 6 compares MLP, DynaMLP, and ShareMLP at matched FFN parameter budgets. At the $1\times$ budget, ShareMLP already improves over the static MLP; at $2\times$, $4\times$, and $8\times$ budgets, it consistently outperforms DynaMLP, supporting the benefit of sharing weight bases across decoder layers. Appendix Table A6 additionally reports how N affects Meganomaly's performance, parameter count, and FLOPs with PTB.

Generality across Baselines. To evaluate generality beyond Dinomaly2, we integrate ShareMLP and PTB into RD4AD, ViTAD, and Dinomaly. For the convolutional RD4AD, ShareMLP is applied to its 1×1 convolutions, while PTB is not applicable because ResNet has neither a `CLS` token nor positional embeddings. As shown in Table 7, the proposed components consistently improve different baselines, supporting their generality for large-category MUAD.

Routing Visualization. We visualize ShareMLP's routing weights on the first 40 categories of Real-IAD Variety. For each image, the routing weights from 8 decoder layers and 64 shared bases are concatenated into a 512-dimensional vector. As shown in Fig. 4(a), t-SNE reveals clear category-aware clusters, despite no category labels being used for training. In the original routing space, 99.40% of anomalous images have their nearest normal neighbor in the same category, suggesting that anomalies rarely alter routing-based category affiliation. The category-averaged heatmap in

Table 4: Ablation on FFN.

FFN Type	Params	FLOPs	I-AUC	O-AUC	P-AUC	AUPRO
MLP (r=4)	1×	1×	86.34	92.78	93.02	79.21
MLP (r=8)	2×	2×	88.34	93.67	93.60	80.74
MLP (r=16)	4×	4×	89.59	94.69	94.11	81.96
MLP (r=32)	8×	8×	90.64	95.38	94.32	82.84
MoE-top1	8×	1×	87.38	93.23	93.49	80.41
MoE-top2	8×	2×	89.06	94.69	94.06	82.30
DY-Conv	9×	1.125×	88.65	93.99	93.98	81.59
CondConv	9×	1.125×	89.29	94.56	94.20	82.04
KW-Conv	9×	1.125×	90.45	95.23	94.65	83.09
DynaMLP	8×	1×	91.66	95.91	94.98	83.86
ShareMLP	8×	1×	**92.00**	**96.26**	**95.12**	**84.23**
ShareMLP (r=2)	4×	0.5×	91.24	95.93	94.82	83.61
ShareMLP (r=1)	2×	0.25×	89.86	95.35	94.29	82.60

with standard NB as bottleneck. r: expansion ratio, default=4. FFN Params and FLOPs are relative to base MLP.

Table 5: Ablation on PTB design.

d_t	PE	Sep.	NF	I-AUC	O-AUC	P-AUC	AUPRO
$4d$				92.00	96.26	95.12	84.23
$4d$	✓			92.22	96.26	95.10	84.18
32				88.43	93.27	93.46	78.63
32	✓			93.65	97.22	95.44	84.33
32	✓	✓		93.58	97.10	**95.49**	**84.74**
32	✓	✓	✓	**93.99**	**97.34**	95.46	84.59
16	✓	✓	✓	93.93	97.22	95.30	83.56
48	✓	✓	✓	93.81	97.17	95.41	84.64
64	✓	✓	✓	93.33	96.69	95.39	84.80

with ShareMLP as FFN. d_t: hidden dim. PE: positional embedding. Sep.: separate `CLS` MLP. NF: noise-free `CLS` MLP.

Table 6: MLP, DynaMLP, and ShareMLP at matched parameter budgets.

FFN	Params	I-AUC	O-AUC	P-AUC	AUPRO
MLP	1×	86.34	92.78	93.02	79.21
ShareMLP (N=8)	1×	**87.47**	**93.50**	**93.40**	**80.02**
DynaMLP (K=2)	2×	88.27	93.85	93.69	80.83
ShareMLP (N=16)	2×	**89.67**	**95.02**	**94.16**	**82.07**
DynaMLP (K=4)	4×	90.18	95.10	94.42	82.48
ShareMLP (N=32)	4×	**90.81**	**95.51**	**94.69**	**83.10**
DynaMLP (K=8)	8×	91.66	95.91	94.98	83.86
ShareMLP (N=64)	8×	**92.00**	**96.26**	**95.12**	**84.23**

with standard NB as bottleneck.

Table 7: Plug-and-play generality of proposed components.

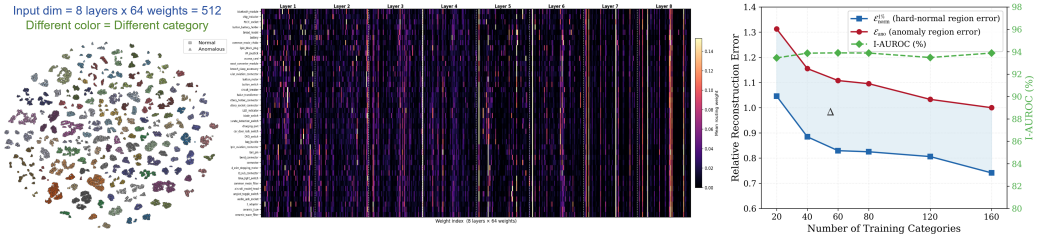
Method	ShareMLP	PTB	I-AUC	O-AUC	P-AUC	AUPRO
RD4AD			72.0	76.7	88.8	68.8
(Deng & Li, 2022)	✓		**76.4**	**85.9**	**89.8**	**71.0**
ViTAD			78.3	83.6	90.9	70.3
(Zhang et al., 2025b)	✓		85.2	91.5	92.9	**76.4**
	✓	✓	**87.0**	**92.6**	**93.6**	76.0
Dinomaly(v1)			87.0	92.5	93.5	79.5
(Guo et al., 2025b)	✓		90.0	95.0	94.5	82.5
	✓	✓	**93.3**	**97.1**	**95.3**	**83.9**

Fig. 4(b) further shows distinct activation patterns across categories, consistent with ShareMLP learning implicit category-specific reconstruction pathways.

Category Scaling Behavior. We repeat the controlled experiment from Sec. 3.1 using Meganomaly-S. As shown in Fig. 4(c), both $\mathcal{E}_{\text{norm}}$ and $\mathcal{E}_{\text{ano}}$ errors decrease together as category count grows, keeping the reconstruction gap and I-AUROC stable. Appendix Fig. A1 further separates the category-scaling effects of ShareMLP and PTB.

Computation, Speed, and Model. Table A7 compares Meganomaly at different model scales. Meganomaly-S already surpasses Dinomaly2-B by +4.96% I-AUROC while using $4\times$ fewer FLOPs and running $2.4\times$ faster (581 FPS). Meganomaly-B has comparable FLOPs to Dinomaly2-B but improves I-AUROC by +5.52%. Table A8 further shows that Meganomaly is robust to backbone choice and improves consistently with stronger encoders.

Additional localization visualizations and per-category results are provided in Appendix A.5.



(a) t-SNE of routing weights (b) Heatmap of routing weights (c) Scaling behavior of Meganomaly

Figure 4: Routing behavior and category-scaling analysis. (a) t-SNE visualization of routing vectors on the first 40 categories of Real-IAD Variety. (b) Mean routing vectors of each category visualized as a heatmap. (c) Meganomaly maintains a relatively stable reconstruction gap and I-AUROC.

5 Conclusion

We identified capacity saturation as a key failure mode beyond over-generalization in large-category multi-class UAD. Motivated by this finding, we proposed Meganomaly, a simple approach that expands effective capacity through input-conditioned weights while controlling information flow. Its improvements across benchmarks support capacity expansion as a practical way to alleviate this limitation. We hope our findings encourage further study and inspire more effective and efficient methods for large-scale UAD. Looking forward, promising directions include developing more parameter-efficient mechanisms for capacity expansion, as well as extending large-category UAD under few-shot, open-vocabulary, or continual learning settings.

AI USE STATEMENT

Generative AI tools were used to assist with language polishing and LaTeX composing. All AI-assisted text and derivations were manually reviewed and checked for correctness by the authors. The authors take responsibility for the final content of this work, including content produced with the aid of generative AI.

REFERENCES

Samet Akcay, Amir Atapour-Abarghouei, and Toby P Breckon. Ganomaly: Semi-supervised anomaly detection via adversarial training. In *Asian conference on computer vision*, pp. 622–637. Springer, 2018.

Paul Bergmann, Michael Fauser, David Sattlegger, and Carsten Steger. MVTec AD–A comprehensive real-world dataset for unsupervised anomaly detection. In *Proceedings of the IEEE/CVF conference on computer vision and pattern recognition*, pp. 9592–9600, 2019.

Mathilde Caron, Hugo Touvron, Ishan Misra, Hervé Jégou, Julien Mairal, Piotr Bojanowski, and Armand Joulin. Emerging properties in self-supervised vision transformers. In *Proceedings of the IEEE/CVF international conference on computer vision*, pp. 9650–9660, 2021.

Yinpeng Chen, Xiyang Dai, Mengchen Liu, Dongdong Chen, Lu Yuan, and Zicheng Liu. Dynamic convolution: Attention over convolution kernels. In *Proceedings of the IEEE/CVF conference on computer vision and pattern recognition*, pp. 11030–11039, 2020.

Timothée Darcet, Maxime Oquab, Julien Mairal, and Piotr Bojanowski. Vision transformers need registers. In *International Conference on Learning Representations*, 2024.

Thomas Defard, Aleksandr Setkov, Angelique Loesch, and Romaric Audigier. PaDiM: A patch distribution modeling framework for anomaly detection and localization. In *International Conference on Pattern Recognition*, pp. 475–489. Springer, 2021.

Hanqiu Deng and Xingyu Li. Anomaly detection via reverse distillation from one-class embedding. In *Proceedings of the IEEE/CVF Conference on Computer Vision and Pattern Recognition*, pp. 9737–9746, 2022.

Alexey Dosovitskiy, Lucas Beyer, Alexander Kolesnikov, Dirk Weissenborn, Xiaohua Zhai, Thomas Unterthiner, Mostafa Dehghani, Matthias Minderer, G Heigold, S Gelly, et al. An image is worth 16x16 words: Transformers for image recognition at scale. In *International Conference on Learning Representations*, 2021.

Lei Fan, Dongdong Fan, Zhiguang Hu, Yiwen Ding, Donglin Di, Kai Yi, Maurice Pagnucco, and Yang Song. MANTA: A large-scale multi-view and visual-text anomaly detection dataset for tiny objects. In *Proceedings of the Computer Vision and Pattern Recognition Conference*, pp. 25518–25527, 2025a.

Lei Fan, Junjie Huang, Donglin Di, Anyang Su, Tianyou Song, Maurice Pagnucco, and Yang Song. Salvaging the overlooked: Leveraging class-aware contrastive learning for multi-class anomaly detection. In *Proceedings of the IEEE/CVF International Conference on Computer Vision*, pp. 21419–21428, 2025b.

William Fedus, Barret Zoph, and Noam Shazeer. Switch transformers: Scaling to trillion parameter models with simple and efficient sparsity. *Journal of Machine Learning Research*, 23(120):1–39, 2022.

Bin-Bin Gao. Learning to detect multi-class anomalies with just one normal image prompt. In *European Conference on Computer Vision*, pp. 454–470. Springer, 2024a.

Bin-Bin Gao. MetaUAS: Universal anomaly segmentation with one-prompt meta-learning. *Advances in Neural Information Processing Systems*, 37:39812–39836, 2024b.

Denis Gudovskiy, Shun Ishizaka, and Kazuki Kozuka. CFlow-AD: Real-time unsupervised anomaly detection with localization via conditional normalizing flows. In *Proceedings of the IEEE/CVF Winter Conference on Applications of Computer Vision*, pp. 98–107, 2022.

Jia Guo, Shuai Lu, Lize Jia, Weihang Zhang, and Huiqi Li. Encoder-decoder contrast for unsupervised anomaly detection in medical images. *IEEE transactions on medical imaging*, 43(3): 1102–1112, 2023a.

Jia Guo, Shuai Lu, Lize Jia, Weihang Zhang, and Huiqi Li. Recontrast: Domain-specific anomaly detection via contrastive reconstruction. In *Advances in Neural Information Processing Systems (NeurIPS)*, volume 36, pp. 10721–10740, 2023b.

Jia Guo, Shuai Lu, Lei Fan, Zelin Li, Donglin Di, Yang Song, Weihang Zhang, Wenbing Zhu, Hong Yan, Fang Chen, et al. One Dinomaly2 detect them all: A unified framework for full-spectrum unsupervised anomaly detection. *arXiv preprint arXiv:2510.17611*, 2025a.

Jia Guo, Shuai Lu, Weihang Zhang, Fang Chen, Huiqi Li, and Hongen Liao. Dinomaly: The less is more philosophy in multi-class unsupervised anomaly detection. In *Proceedings of the Computer Vision and Pattern Recognition Conference*, pp. 20405–20415, 2025b.

Haoyang He, Yuhu Bai, Jiangning Zhang, Qingdong He, Hongxu Chen, Zhenye Gan, Chengjie Wang, Xiangtai Li, Guanzhong Tian, and Lei Xie. MambaAD: Exploring state space models for multi-class unsupervised anomaly detection. *Advances in Neural Information Processing Systems*, 37:71162–71187, 2024a.

Haoyang He, Jiangning Zhang, Hongxu Chen, Xuhai Chen, Zhishan Li, Xu Chen, Yabiao Wang, Chengjie Wang, and Lei Xie. A diffusion-based framework for multi-class anomaly detection. In *Proceedings of the AAAI Conference on Artificial Intelligence*, volume 38, pp. 8472–8480, 2024b.

Jeeho Hyun, Sangyun Kim, Giyoung Jeon, Seung Hwan Kim, Kyunghoon Bae, and Byung Jun Kang. Reconpatch: Contrastive patch representation learning for industrial anomaly detection. In *Proceedings of the IEEE/CVF Winter Conference on Applications of Computer Vision*, pp. 2052–2061, 2024.

Robert A Jacobs, Michael I Jordan, Steven J Nowlan, and Geoffrey E Hinton. Adaptive mixtures of local experts. *Neural computation*, 3(1):79–87, 1991.

Jongheon Jeong, Yang Zou, Taewan Kim, Dongqing Zhang, Avinash Ravichandran, and Onkar Dabeer. WinCLIP: Zero-/few-shot anomaly classification and segmentation. In *Proceedings of the IEEE/CVF Conference on Computer Vision and Pattern Recognition*, pp. 19606–19616, 2023.

Angelos Katharopoulos, Apoorv Vyas, Nikolaos Pappas, and François Fleuret. Transformers are RNNs: Fast autoregressive transformers with linear attention. In *International conference on machine learning*, pp. 5156–5165. PMLR, 2020.

Alex Kendall and Yarin Gal. What uncertainties do we need in bayesian deep learning for computer vision? *Advances in neural information processing systems*, 30, 2017.

Sungwook Lee, Seunghyun Lee, and Byung Cheol Song. CFA: Coupled-hypersphere-based feature adaptation for target-oriented anomaly localization. *IEEE Access*, 10:78446–78454, 2022.

Dmitry Lepikhin, HyoukJoong Lee, Yuanzhong Xu, Dehao Chen, Orhan Firat, Yanping Huang, Maxim Krikun, Noam Shazeer, and Zhifeng Chen. GShard: Scaling giant models with conditional computation and automatic sharding. In *International Conference on Learning Representations*, 2021.

Chao Li and Anbang Yao. KernelWarehouse: Rethinking the design of dynamic convolution. In *Proceedings of the 41st International Conference on Machine Learning*, volume 235 of *Proceedings of Machine Learning Research*, pp. 29201–29221. PMLR, 2024.

Chao Li, Aojun Zhou, and Anbang Yao. Omni-dimensional dynamic convolution. In *International Conference on Learning Representations*, 2022.

Chaoming Li, Guoqing Yu, and Wenwen Ye. Hiprotoad: Feature reconstruction guided by cluster-separated hierarchical prototypes for multi-class unsupervised anomaly detection. *IEEE Access*, 2026.

Chun-Liang Li, Kihyuk Sohn, Jinsung Yoon, and Tomas Pfister. Cutpaste: Self-supervised learning for anomaly detection and localization. In *Proceedings of the IEEE/CVF Conference on Computer Vision and Pattern Recognition*, pp. 9664–9674, 2021.

Yiting Li, Adam Goodge, Fayao Liu, and Chuan-Sheng Foo. PromptAD: Zero-shot anomaly detection using text prompts. In *Proceedings of the IEEE/CVF Winter Conference on Applications of Computer Vision*, pp. 1093–1102, 2024.

Hai Ling, Jia Guo, Zhulin Tao, Yunkang Cao, Donglin Di, Hongyan Xu, Xiu Su, Yang Song, and Lei Fan. ADNet: A large-scale and extensible multi-domain benchmark for anomaly detection across 380 real-world categories. *arXiv preprint arXiv:2511.20169*, 2025.

Tongtong Liu, Hongxia Gao, Yuxuan Tan, Jinpeng Li, and Jinhui Zhao. Entropy-increasing linear attention for multi-class unsupervised anomaly detection. *Pattern Recognition*, pp. 113089, 2026.

Zhikang Liu, Yiming Zhou, Yuansheng Xu, and Zilei Wang. SimpleNet: A simple network for image anomaly detection and localization. In *Proceedings of the IEEE/CVF conference on computer vision and pattern recognition*, pp. 20402–20411, 2023.

Ruiying Lu, YuJie Wu, Long Tian, Dongsheng Wang, Bo Chen, Xiyang Liu, and Ruimin Hu. Hierarchical vector quantized transformer for multi-class unsupervised anomaly detection. *Advances in Neural Information Processing Systems*, 36:8487–8500, 2023.

Wei Luo, Yunkang Cao, Haiming Yao, Xiaotian Zhang, Jianan Lou, Yuqi Cheng, Weiming Shen, and Wenyong Yu. Exploring intrinsic normal prototypes within a single image for universal anomaly detection. In *Proceedings of the Computer Vision and Pattern Recognition Conference*, pp. 9974–9983, 2025.

Amira Ben Mabrouk and Ezzeddine Zagrouba. Abnormal behavior recognition for intelligent video surveillance systems: A review. *Expert Systems with Applications*, 91:480–491, 2018.

Shiyuan Meng, Wenchao Meng, Qihang Zhou, Shizhong Li, Weiye Hou, and Shibo He. MoEAD: A parameter-efficient model for multi-class anomaly detection. In *European Conference on Computer Vision*, pp. 345–361. Springer, 2024.

Maxime Oquab, Timothée Darcet, Théo Moutakanni, Huy Vo, Marc Szafraniec, Vasil Khalidov, Pierre Fernandez, Daniel Haziza, Francisco Massa, Alaaeldin El-Nouby, et al. DINOv2: Learning robust visual features without supervision. *Transactions on Machine Learning Research Journal*, pp. 1–31, 2024.

Carlos Riquelme, Joan Puigcerver, Basil Mustafa, Maxim Neumann, Rodolphe Jenatton, André Susano Pinto, Daniel Keysers, and Neil Houlsby. Scaling vision with sparse mixture of experts. In *Advances in Neural Information Processing Systems*, volume 34, pp. 8583–8595, 2021.

Karsten Roth, Latha Pemula, Joaquin Zepeda, Bernhard Schölkopf, Thomas Brox, and Peter Gehler. Towards total recall in industrial anomaly detection. In *Proceedings of the IEEE/CVF Conference on Computer Vision and Pattern Recognition*, pp. 14318–14328, 2022.

Mohammadreza Salehi, Niousha Sadjadi, Soroosh Baselizadeh, Mohammad H Rohban, and Hamid R Rabiee. Multiresolution knowledge distillation for anomaly detection. In *Proceedings of the IEEE/CVF conference on computer vision and pattern recognition*, pp. 14902–14912, 2021.

Pedro Savarese and Michael Maire. Learning implicitly recurrent CNNs through parameter sharing. In *International Conference on Learning Representations*, 2019.

Noam Shazeer, Azalia Mirhoseini, Krzysztof Maziarz, Andy Davis, Quoc Le, Geoffrey Hinton, and Jeff Dean. Outrageously large neural networks: The sparsely-gated mixture-of-experts layer. In *International Conference on Learning Representations*, 2017.

Nitish Srivastava, Geoffrey Hinton, Alex Krizhevsky, Ilya Sutskever, and Ruslan Salakhutdinov. Dropout: a simple way to prevent neural networks from overfitting. *The journal of machine learning research*, 15(1):1929–1958, 2014.

Peng Tang, Xiaobin Hu, Tingcheng Li, Yang Nan, Tobias Lasser, and Hongwei Bran Li. Shortcut-breaker: Low-rank noisy bottleneck and frequency filtering block for multi-class unsupervised anomaly detection. *arXiv preprint arXiv:2510.18342*, 2025.

Piotr Teterwak, Soren Nelson, Nikoli Dryden, Dina Bashkirova, Kate Saenko, and Bryan A Plummer. Learning to compose superweights for neural parameter allocation search. In *2024 IEEE/CVF Winter Conference on Applications of Computer Vision (WACV)*, pp. 2739–2748. IEEE, 2024.

Chengjie Wang, Wenbing Zhu, Bin-Bin Gao, Zhenye Gan, Jiangning Zhang, Zhihao Gu, Shuguang Qian, Mingang Chen, and Lizhuang Ma. Real-IAD: A real-world multi-view dataset for benchmarking versatile industrial anomaly detection. In *Proceedings of the IEEE/CVF Conference on Computer Vision and Pattern Recognition*, pp. 22883–22892, 2024.

Qishan Wang, Haofeng Wang, Shuyong Gao, Jia Guo, Li Xiong, Jiaqi Li, Dengxuan Bai, and Wenqiang Zhang. Collaborative reconstruction and repair for multi-class industrial anomaly detection. *arXiv preprint arXiv:2512.11401*, 2025a.

Xiaolei Wang, Xiaoyang Wang, Huihui Bai, Eng Gee Lim, and Jimin Xiao. DecAD: Decoupling anomalies in latent space for multi-class unsupervised anomaly detection. In *Proceedings of the IEEE/CVF International Conference on Computer Vision*, pp. 21568–21577, 2025b.

Yuexin Wang, Xiaolei Wang, Yizheng Gong, and Jimin Xiao. Normal-abnormal guided generalist anomaly detection. *Advances in Neural Information Processing Systems*, 38:62560–62585, 2026.

Mitchell Wortsman, Tim Dettmers, Luke Zettlemoyer, Ari Morcos, Ali Farhadi, and Ludwig Schmidt. Stable and low-precision training for large-scale vision-language models. *Advances in Neural Information Processing Systems*, 36:10271–10298, 2023.

Tiange Xiang, Yixiao Zhang, Yongyi Lu, Alan Yuille, Chaoyi Zhang, Weidong Cai, and Zongwei Zhou. Exploiting structural consistency of chest anatomy for unsupervised anomaly detection in radiography images. *IEEE Transactions on Pattern Analysis and Machine Intelligence*, 46(9): 6070–6081, 2024.

Brandon Yang, Gabriel Bender, Quoc V Le, and Jiquan Ngiam. CondConv: Conditionally parameterized convolutions for efficient inference. In *Advances in Neural Information Processing Systems*, volume 32, 2019.

Yu Yao, Xizi Wang, Mingze Xu, Zelin Pu, Yuchen Wang, Ella Atkins, and David J Crandall. DoTA: Unsupervised detection of traffic anomaly in driving videos. *IEEE transactions on pattern analysis and machine intelligence*, 45(1):444–459, 2022.

Haonan Yin, Guanlong Jiao, Qianhui Wu, Borje F Karlsson, Biqing Huang, and Chin Yew Lin. LafitE: Latent diffusion model with feature editing for unsupervised multi-class anomaly detection. *arXiv preprint arXiv:2307.08059*, 2023.

Zhiyuan You, Lei Cui, Yujun Shen, Kai Yang, Xin Lu, Yu Zheng, and Xinyi Le. A unified model for multi-class anomaly detection. *Advances in Neural Information Processing Systems*, 35:4571–4584, 2022.

Jiawei Yu, Ye Zheng, Xiang Wang, Wei Li, Yushuang Wu, Rui Zhao, and Liwei Wu. Fastflow: Unsupervised anomaly detection and localization via 2d normalizing flows. *arXiv preprint arXiv:2111.07677*, 2021.

Vitjan Zavrtanik, Matej Kristan, and Danijel Skoč aj. DRAEM-a discriminatively trained reconstruction embedding for surface anomaly detection. In *Proceedings of the IEEE/CVF International Conference on Computer Vision*, pp. 8330–8339, 2021.

Hui Zhang, Zheng Wang, Dan Zeng, Zuxuan Wu, and Yu-Gang Jiang. DiffusionAD: Norm-guided one-step denoising diffusion for anomaly detection. *IEEE Transactions on Pattern Analysis and Machine Intelligence*, 2025a.

Jiangning Zhang, Haoyang He, Zhenye Gan, Qingdong He, Yuxuan Cai, Zhucun Xue, Yabiao Wang, Chengjie Wang, Lei Xie, and Yong Liu. ADer: A Comprehensive Benchmark for Multi-class Visual Anomaly Detection. *arXiv preprint arXiv:2406.03262*, 2024.

Jiangning Zhang, Xuhai Chen, Yabiao Wang, Chengjie Wang, Yong Liu, Xiangtai Li, Ming-Hsuan Yang, and Dacheng Tao. Exploring plain vit features for multi-class unsupervised visual anomaly detection. *Computer Vision and Image Understanding*, 253:104308, 2025b. ISSN 1077-3142.

Xuan Zhang, Shiyu Li, Xi Li, Ping Huang, Jiulong Shan, and Ting Chen. DeSTSeg: Segmentation guided denoising student-teacher for anomaly detection. In *Proceedings of the IEEE/CVF Conference on Computer Vision and Pattern Recognition*, pp. 3914–3923, 2023.

Ying Zhao. OmniAL: A unified CNN framework for unsupervised anomaly localization. In *Proceedings of the IEEE/CVF Conference on Computer Vision and Pattern Recognition*, pp. 3924–3933, 2023.

Yibo Zhong, Jinman Zhao, and Yao Zhou. Low-rank interconnected adaptation across layers. In *Findings of the Association for Computational Linguistics: ACL 2025*, pp. 17005–17029, 2025.

Jinghao Zhou, Chen Wei, Huiyu Wang, Wei Shen, Cihang Xie, Alan Yuille, and Tao Kong. Image BERT pre-training with online tokenizer. In *International Conference on Learning Representations*, 2022.

Wenbing Zhu, Chengjie Wang, Bin-Bin Gao, Jiangning Zhang, Guannan Jiang, Jie Hu, Zhenye Gan, Lidong Wang, Ziqing Zhou, Jianghui Zhang, et al. Real-IAD Variety: Pushing industrial anomaly detection dataset to a modern era. *Pattern Recognition*, pp. 113354, 2026.

Yang Zou, Jongheon Jeong, Latha Pemula, Dongqing Zhang, and Onkar Dabeer. Spot-the-difference self-supervised pre-training for anomaly detection and segmentation. In *European Conference on Computer Vision*, pp. 392–408. Springer, 2022.

A Appendix

A.1 Extended Related Work

Unsupervised Anomaly Detection. Image UAD has evolved through several complementary paradigms. *Feature reconstruction* (or distillation) methods (Deng & Li, 2022; Salehi et al., 2021; Hyun et al., 2024) train a student decoder to reconstruct features extracted by a pre-trained encoder, detecting anomalies where reconstruction fails. *Synthetic anomaly* methods (Li et al., 2021; Zavrtanik et al., 2021; Zhang et al., 2023; Liu et al., 2023) generate artificial defects on normal images and convert UAD into a supervised segmentation task, but their effectiveness depends heavily on how well the synthetic anomalies approximate real ones. *Memory-based* methods (Defard et al., 2021; Roth et al., 2022; Lee et al., 2022) store normal features from pre-trained networks and detect anomalies via distribution matching at inference. Such methods incur substantial memory and computation costs that scale with training set size. Recent works have also explored normalizing flows (Gudovskiy et al., 2022; Yu et al., 2021) and diffusion models (He et al., 2024b; Zhang et al., 2025a) for modeling normal distributions. Few-shot and zero-shot UAD approaches leverage vision-language models or meta-learning to compensate for scarce visual data (Jeong et al., 2023; Li et al., 2024; Gao, 2024b; Wang et al., 2026). Among these paradigms, feature reconstruction has emerged as particularly suitable for multi-class settings due to its simplicity and scalability, and forms the basis of our work.

Multi-Class UAD. UniAD (You et al., 2022) first formalized the multi-class setting and proposed to prevent identity mapping (over-generalization). Subsequent works tackled over-generalization from various angles: OmniAL (Zhao, 2023) via synthetic anomalies, LafitE (Yin et al., 2023) and DiAD (He et al., 2024b) via diffusion models, MoEAD(Meng et al., 2024) via patch-level mixture-of-experts, ReContrast (Guo et al., 2023b) via contrastive cross-reconstruction, CCL(Fan

et al., 2025b) via class-aware representation learning, DecAD (Wang et al., 2025b) via decoupling anomalies in latent space, ViTAD (Zhang et al., 2025b) via Vision Transformer (ViT) features, and MambaAD (He et al., 2024a) via state space models. Despite these efforts, a notable performance gap persisted between multi-class and single-class models. Dinomaly (Guo et al., 2025b) was the first to close this gap, demonstrating that simple components—dropout-based bottleneck, linear attention, and loose reconstruction—suffice when built upon foundational ViT features. The simple framework of ViTAD and Dinomaly has inspired several extensions: INP-Former (Luo et al., 2025) and HiProtoAD (Li et al., 2026) introduces learnable tokens as normal prototypes;EILA-AD (Liu et al., 2026) and ShortcutBreaker (Tang et al., 2025) refine Linear Attention and Noisy Bottleneck to further mitigate identity mapping.; Dinomaly+(Zhu et al., 2026) and CRR(Wang et al., 2025a) propose to train an extra segmentation module using synthetic anomalies; Dinomaly2 (Guo et al., 2025a) introduces context-aware recentering to resolve multi-class feature confusion. While these methods achieve impressive results on small-scale benchmarks, they share a common limitation: their performance degrades substantially when scaling to hundreds of categories.

Conditional and Dynamic Computation. Mixture of Experts (MoE) (Jacobs et al., 1991; Shazeer et al., 2017; Fedus et al., 2022) is a well-established paradigm for scaling model capacity, achieving success in large language models (Fedus et al., 2022; Lepikhin et al., 2021) and vision models (Riquelme et al., 2021). However, its per-token routing poses challenges for UAD: tokens within the same image may be dispatched to different experts, potentially allowing anomalous tokens to exploit experts specialized for other categories. An alternative line increases capacity through *dynamic weights*, where network parameters are composed conditioned on the input. Existing dynamic weight methods are predominantly designed for convolutional architectures. CondConv (Yang et al., 2019) and DY-Conv (Chen et al., 2020) combine convolutional kernels using input-dependent coefficients, while ODConv (Li et al., 2022) extends dynamic modulation across kernel, spatial, and channel dimensions. Parameter sharing improves parameter utilization across layers. Savarese & Maire (2019) and SuperWeights(Teterwak et al., 2024) construct layer weights from shared templates using learned, input-independent coefficients. KWH (Li & Yao, 2024) dynamically assembles partitioned convolutional cells from shared warehouses, whereas Lily (Zhong et al., 2025) dynamically combines shared LoRA experts for parameter-efficient fine-tuning. These methods address diverse objectives, from representation learning to parameter-efficient adaptation. Building on these ideas, we develop a simple design for expanding network capacity in large-category MUAD and adopt cross-layer weight sharing to maximize capacity efficiency.

A.2 Preliminary: Reconstruction-Based UAD

Following ViTAD (Zhang et al., 2025b), Dinomaly (Guo et al., 2025b) and Dionmaly2 (Guo et al., 2025a), we adopt a feature-reconstruction framework consisting of a frozen pre-trained encoder, a trainable bottleneck, and a trainable decoder.

Given an input image $\mathbf{x} \in \mathbb{R}^{H\times W\times C}$, a pre-trained Vision Transformer (ViT) (Dosovitskiy et al., 2021) $\mathcal{E}$ with L layers extracts hierarchical features. We collect features from L_e middle layers indexed by $\mathcal{M}$:

$$\mathbf{F}^* = \{\mathbf{f}_i \mid i \in \mathcal{M}\}, \tag{5}$$

where $\mathbf{f}_i = [\mathbf{f}_i^{cls}; \mathbf{f}_i^{patch}] \in \mathbb{R}^{(1+N)\times d}$ consists of a `CLS` token $\mathbf{f}_i^{cls} \in \mathbb{R}^d$ and N patch tokens $\mathbf{f}_i^{patch} \in \mathbb{R}^{N\times d}$. By default, we use ViT-Base (L=12) with $\mathcal{M}$=$\{3, 4, \ldots, 10\}$ (L_e=8). The encoder remains frozen throughout training.

The selected features are aggregated and passed through a noisy bottleneck $\mathcal{B}$, implemented as an MLP with Dropout (Srivastava et al., 2014):

$$\mathbf{z} = \mathcal{B}\Big(\sum \mathbf{F}^*\Big). \tag{6}$$

The decoder $\mathcal{D}$ consists of L_d Transformer layers, each containing a Linear Attention (Katharopoulos et al., 2020) block and a feed-forward MLP block. It reconstructs the encoder's intermediate features:

$$\hat{\mathbf{F}} = \mathcal{D}(\mathbf{z}) = \{\hat{\mathbf{f}}_j \mid j \in \{1, \ldots, L_d\}\}, \tag{7}$$

where L_d=L_e by default.

Encoder and decoder layers are divided into $|\mathcal{G}|$=2 semantic groups (Guo et al., 2025b):

$$\mathbf{g}_k = \sum_{i \in \mathcal{G}_k} \mathbf{f}_i^*, \quad \hat{\mathbf{g}}_k = \sum_{j \in \mathcal{G}_k} \hat{\mathbf{f}}_j, \quad k \in \{1, 2\}, \tag{8}$$

where $\mathcal{G}$=$\{\{1, 2, 3, 4\}, \{5, 6, 7, 8\}\}$ partitions the layers into shallow and deep groups. The model is trained on normal samples to minimize the cosine distance between original and reconstructed group features:

$$\mathcal{L}_{recon} = \sum_{k \in \{1,2\}} d_{\cos}\big(\mathcal{F}(\mathbf{g}_k),\ \mathcal{F}(\hat{\mathbf{g}}_k)\big), \tag{9}$$

where $\mathcal{F}$ denotes flattening and $d_{\cos}$ denotes cosine distance.

A.3 Implementation Details

Following the Dinomaly series (Guo et al., 2025b;a), we use DINOv2-ViT-B/14 with registers (DINOv2R-Base) (Oquab et al., 2024; Darcet et al., 2024) as the frozen encoder by default. Features from the middle 8 layers of ViT-B serve as reconstruction targets and bottleneck inputs. The hard-mining cosine loss and context-aware recentering are also adopted. The MegaDecoder contains 8 layers. ShareMLP maintains two weight pools shared across all decoder layers, one for each Linear in the MLP, with N=64 bases per pool. Each layer uses a single linear router $\mathbb{R}^d \to \mathbb{R}^{64}$, whose softmax outputs provide the same mixing coefficients for both pools. For PTB, the compressed dimension is d_t=32, the Dropout rate is 0.4, and $\mathbf{PE}$ directly uses the encoder's positional embedding. For well established datasets (MVTec-AD, VisA, Real-IAD), we follow Dinomaly to use 392×392 input. For newer datasets with more than 30 categories (Real-IAD Variety, ADNet, MANTA), we use 280×280 for efficiency. StableAdamW optimizer (Wortsman et al., 2023) is utilized with lr=2×10^{-3}, β=(0.9,0.999), and wd (weight decay)=1×10^{-4}. Under the MUAD setting, the model is trained with the batch size of 16 for 100,000 iterations by default and 40,000 iterations for small datasets. Experiments were run on NVIDIA GeForce RTX3090/4090 GPUs with PyTorch 2.9.0. Code will be available upon acceptance.

For the category-scaling diagnostic experiments in Fig. 1(b), Fig. 4(c), and Fig. A1, we use DINOv2-ViT-S/14 with registers (DINOv2R-Small) as the frozen encoder for efficiency. For comparison across different category configurations, we train each model for a sufficiently long schedule (up to 200,000 iters) to ensure adequate exposure to all training images, providing full convergence before overfitting. StableAdamW optimizer is utilized with lr=2×10^{-3}, β=(0.9,0.999), and wd=1×10^{-4}.

A.4 Additional Experiments

We provide additional results on small-scale benchmarks and examine the effects of bottleneck dropout, weight-pool size, model scale, encoder choice, and random-seed stability.

Small-scale benchmarks. Table A1 shows that Meganomaly remains competitive on MVTec-AD and VisA, where image-level detection is already near saturation. On Uni-Medical, it improves image-level detection and pixel-level AP over Dinomaly2, extending its benefits beyond industrial inspection.

Stability across random seeds. Across five runs of Meganomaly-S on Real-IAD Variety, the small standard deviations across metrics indicate stable performance across random seeds (Table A2).

Simple bottlenecks. Table A3 shows that ShareMLP can improve I-AUROC by 6.57 and 5.45 points with a single Linear layer and a plain MLP as the bottleneck, respectively. These gains show that its benefit does not depend on the dedicated information constraints of NB or PTB.

Additional Design Choices. Table A4 examines router network, router input, routing balance loss (Fedus et al., 2022), finer-grained weight partition into $d \times d$ blocks (Li & Yao, 2024), and the contrasting-driven routing function with temperature annealing (Li & Yao, 2024). A two-layer router provides only marginal gains. Replacing the `CLS` token with mean-pooled patch features reduces performance with a linear router, but a two-layer router can easily recovers this loss. The remaining additions also yield only marginal gains, with no single variant consistently performing best across metrics. We therefore retain the simpler ShareMLP design by default.

Bottleneck dropout. Table A5 shows that PTB maintains I-AUROC above 93.5% across dropout rates from 0.2 to 0.6, whereas NB is more sensitive to this choice. Increasing dropout alone does not consistently improve performance, suggesting that the structure of the information bottleneck matters beyond the amount of stochastic masking.

Weight-pool size. At the same reported parameter count as the static MLP, ShareMLP with N=8 improves I-AUROC from 90.10% to 91.54% (Table A6). Increasing N provides further gains with modest growth in FLOPs, while the improvement from 64 to 96 bases is small. We therefore use N=64 to balance performance and parameter cost.

Model scale. Table A7 shows that Meganomaly-S already outperforms Dinomaly2-B while requiring substantially fewer FLOPs and achieving higher throughput. Larger Meganomaly variants further improve detection and localization, although the gains diminish as computational cost increases.

Encoder choice. Table A8 shows that Meganomaly works with several pre-trained ViT encoders. DINOv2-based encoders yield higher detection and localization scores than DINO and iBOT, while DINOv2-B and DINOv2R-B perform similarly, indicating that the framework does not depend on register tokens.

Category Scaling. Figure A1 compares baseoine (Dinomaly2) with ShareMLP, PTB, and their combination (Meganomaly). The baseline exhibits normal-reconstruction saturation while anomaly reconstruction continues to improve, progressively narrowing the reconstruction gap. ShareMLP sustains improvements in normal reconstruction, but also facilitates anomaly reconstruction, leaving a residual decline in detection performance. PTB alone retains a reconstruction gap but does not resolve normal-side saturation: normal error rebounds after 60 categories and then plateaus, consistent with its role in restricting over-generalization rather than expanding reconstruction capacity. Combining both components preserves the reconstruction gap and maintains stable I-AUROC and P-AUROC, supporting their complementary roles.

Table A1: Results on small-scale benchmarks under the multi-class UAD setting.

Method	Image-level			Pixel-level			
	AUROC	AP	F_1-max	AUROC	AP	F_1-max	AUPRO
MVTec-AD (Bergmann et al., 2019)							
RD4AD (Deng & Li, 2022)	94.6	96.5	95.2	96.1	48.6	53.8	91.1
SimpleNet (Liu et al., 2023)	95.3	98.4	95.8	96.9	45.9	49.7	86.5
UniAD (You et al., 2022)	96.5	98.8	96.2	96.8	43.4	49.5	90.7
ViTAD (Zhang et al., 2025b)	98.3	99.4	97.3	97.7	55.3	58.7	91.4
MambaAD (He et al., 2024a)	98.6	99.6	97.8	97.7	56.3	59.2	93.1
Dinomaly (Guo et al., 2025b)	99.7	99.8	99.2	**98.4**	**69.3**	**69.2**	94.7
Dinomaly2 (Guo et al., 2025a)	99.8	99.9	99.3	**98.4**	**69.3**	68.9	94.8
Meganomaly	**99.9**	**100.0**	**99.6**	**98.4**	68.4	67.2	**95.3**
VisA (Zou et al., 2022)							
RD4AD (Deng & Li, 2022)	92.4	92.4	89.6	98.1	38.0	42.6	91.8
SimpleNet (Liu et al., 2023)	87.2	87.0	81.8	96.8	34.7	37.8	81.4
UniAD (You et al., 2022)	88.8	90.8	85.8	98.3	33.7	39.0	85.5
ViTAD (Zhang et al., 2025b)	90.5	91.7	86.3	98.2	36.6	41.1	85.1
MambaAD (He et al., 2024a)	94.3	94.5	89.4	98.5	39.4	44.0	91.0
Dinomaly (Guo et al., 2025b)	98.9	99.0	96.4	98.8	**53.8**	55.8	94.5
Dinomaly2 (Guo et al., 2025a)	99.2	**99.3**	97.0	99.1	52.9	**56.4**	95.5
Meganomaly	**99.3**	**99.3**	**97.2**	**99.2**	52.6	54.8	**95.7**
Uni-Medical Zhang et al. (2024)							
SimpleNet (Liu et al., 2023)	77.5	77.7	76.7	94.3	34.4	36.0	77.0
DeSTSeg (Zhang et al., 2023)	78.5	77.0	78.2	65.7	41.7	34.0	35.3
UniAD (You et al., 2022)	79.0	76.1	77.1	96.6	39.3	41.1	86.0
ViTAD (Zhang et al., 2025b)	81.8	80.7	80.0	97.1	48.3	48.2	86.7
MambaAD (He et al., 2024a)	83.9	80.8	81.9	96.8	45.8	47.5	88.2
Dinomaly (Guo et al., 2025b)	84.9	84.1	81.0	96.8	51.7	52.1	85.5
Dinomaly2 (Guo et al., 2025a)	86.7	84.4	82.1	**97.9**	54.7	**55.2**	90.0
Meganomaly	**88.0**	**87.1**	**82.9**	97.8	**56.3**	55.0	**90.4**

Table A2: Meganomaly-S on Real-IAD Variety across five random seeds. All values are percentages; the last row reports the mean and sample standard deviation across runs.

Run	Image-level			Object-level			Pixel-level			
	AUROC	AP	F_1-max	AUROC	AP	F_1-max	AUROC	AP	F_1-max	AUPRO
Run 1	93.99	98.82	96.35	97.34	99.60	98.57	95.46	53.37	54.25	84.59
Run 2	93.89	98.80	96.32	97.32	99.59	98.56	95.44	53.50	54.34	84.48
Run 3	94.09	98.85	96.39	97.43	99.61	98.60	95.48	53.75	54.54	84.60
Run 4	94.06	98.83	96.41	97.29	99.59	98.60	95.50	53.75	54.52	84.74
Run 5	93.97	98.82	96.38	97.29	99.59	98.59	95.47	53.69	54.41	84.51
Mean $\pm$ std	94.00 ± 0.08	98.82 ± 0.02	96.37 ± 0.04	97.33 ± 0.06	99.60 ± 0.01	98.58 ± 0.02	95.47 ± 0.02	53.61 ± 0.17	54.41 ± 0.12	84.58 ± 0.10

Table A3: ShareMLP with simple bottlenecks on Real-IAD Variety. Bottleneck Linear: $384 \to 384$; Bottleneck MLP: $384 \to 256 \to 384$.

Bottleneck	Decoder FFN	I-AUC	O-AUC	P-AUC	AUPRO
Linear	MLP	77.26	86.22	89.34	70.76
	ShareMLP	**83.83**	**90.52**	**91.85**	**77.19**
MLP	MLP	81.61	89.39	91.19	74.85
	ShareMLP	**87.06**	**92.84**	**93.26**	**80.07**

Table A4: Additional design choices for ShareMLP on Real-IAD Variety.

Setting	I-AUC	O-AUC	P-AUC	AUPRO
ShareMLP	92.00	96.26	95.12	84.23
+ two-layer router	92.19	96.29	95.15	84.21
+ mean-patch routing	91.21	95.71	95.00	83.75
+ mean-patch routing & two-layer router	92.19	96.24	95.13	84.27
+ balance loss	92.03	96.04	95.10	84.30
+ weight partition	92.29	96.17	95.23	84.41
+ contrasting-driven router	92.07	96.32	95.22	84.28

with standard NB as bottleneck.

Table A5: Effect of dropout rates in NB and PTB.

$dropout$	NB	PTB	I-AUC	O-AUC	P-AUC	AUPRO
0.2	✓		91.11	96.61	94.90	83.67
0.4	✓		92.00	96.26	95.12	84.23
0.6	✓		88.46	94.54	94.78	83.24
0.2		✓	93.60	97.11	**95.48**	**84.97**
0.4		✓	**93.99**	**97.34**	95.46	84.59
0.6		✓	93.53	97.00	95.09	82.92

with ShareMLP as FFN.

Table A6: Performance, Params, and FLOPs of different weights pool size N in ShareMLP.

	N	FFN Params	Total Params	Total FLOPs	I-AUC	O-AUC	P-AUC	AUPRO
MLP	-	$\times 1$	36.3M	26.2G	90.10	95.38	94.02	82.07
ShareMLP	8	$\times 1$	36.3M	26.5G	91.54	96.13	94.50	82.80
ShareMLP	16	$\times 2$	45.8M	26.7G	92.70	96.84	95.01	83.93
ShareMLP	32	$\times 4$	64.8M	27.0G	93.53	97.17	95.23	84.27
ShareMLP	64	$\times 8$	102.7M	27.6G	93.99	97.34	95.46	84.59
ShareMLP	96	$\times 12$	140.6M	28.2G	94.12	97.44	95.47	84.20

with PTB as bottleneck.

Table A7: Effect of model size. FPS is measured on an NVIDIA RTX 4090 with a batch size of 128.

Model	Params	FLOPs	FPS	I-AUC	O-AUC	P-AUC	AUPRO
Dinomaly2-B	146.6M	106.4G	240	89.03	94.22	94.01	81.76
Meganomaly-S	102.7M	27.6G	581	93.99	97.34	95.46	84.59
Meganomaly-B	408.2M	109.2G	215	94.55	97.75	95.75	85.39
Meganomaly-L	875.9M	285.3G	93	94.78	97.80	95.90	85.89

Table A8: Effect of different backbone foundation model. The linear-probing accuracy of the backbone mode on ImageNet is also presented.

Model	*ImageNet*	I-AUC	O-AUC	P-AUC	AUPRO
DINO-B (Caron et al., 2021)	78.2%	91.92	95.64	94.68	80.17
iBOT-B (Zhou et al., 2022)	79.5%	92.62	95.96	95.13	81.02
DINOv2-B (Oquab et al., 2024)	84.5%	94.52	97.58	95.79	85.55
DINOv2R-B (Darcet et al., 2024)	84.8%	94.55	97.75	95.75	85.39

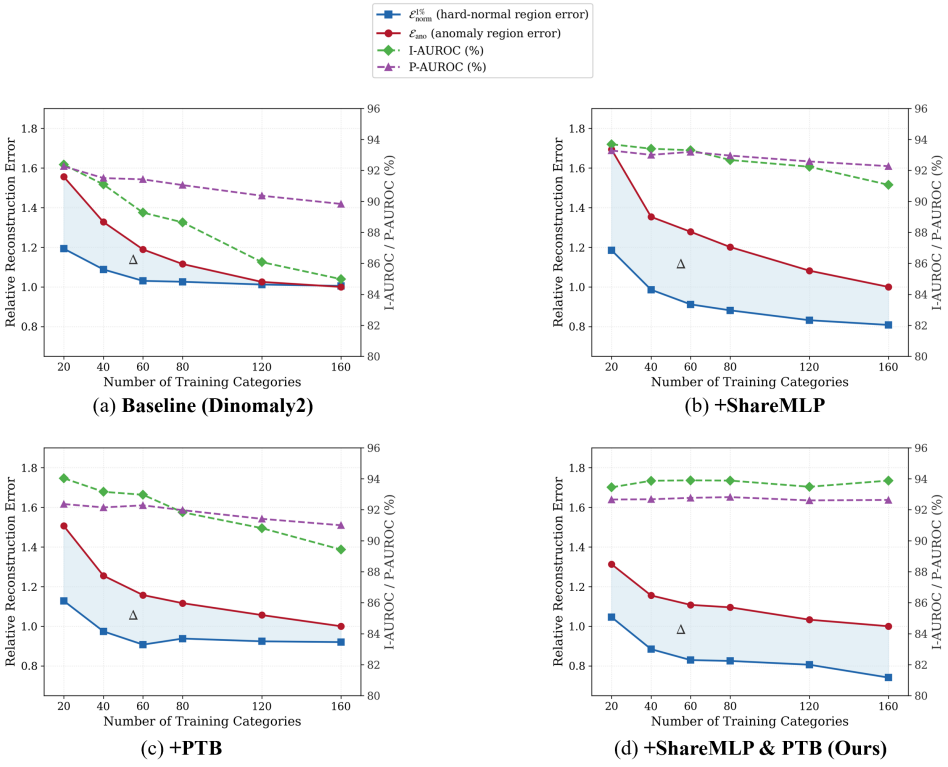


Figure A1: **Component-wise category-scaling behavior on Real-IAD Variety.** Models are trained on 20–160 categories and evaluated on the same fixed first 20-category test set. Reconstruction errors are normalized by each model's anomaly-region error at 160 categories, providing a common reference for comparing trends across models with different absolute error scales.

A.5 Per-Category Results and Qualitative Visualizations

We report the per-category results on all evaluated datasets, followed by qualitative anomaly-localization comparisons. Wide multi-page tables are rotated within portrait PDF pages for readability.

Table A9: Per-category results of Meganomaly-B on Real-IAD Variety. All values are percentages (%).

Category	I-AUROC	I-AP	I-F1	O-AUROC	O-AP	O-F1	P-AUROC	P-AP	P-F1	P-AUPRO
2pin_block_plug	99.25	99.89	99.45	100.00	100.00	100.00	94.59	68.21	64.34	82.82
3_adapter	93.09	98.93	95.87	97.37	99.62	98.51	97.41	46.83	48.88	83.40
3pin_aviation_connector	91.97	98.88	94.31	94.80	99.31	96.45	98.68	73.97	69.69	90.18
4_wire_stepping_motor	85.03	97.80	94.16	89.26	98.46	94.48	75.46	3.41	9.64	48.48
DVD_switch	94.31	98.96	97.74	94.66	98.92	99.50	91.57	53.95	54.51	81.12
D_sub_connector	98.58	99.69	99.18	99.98	100.00	99.75	96.99	60.72	58.97	90.13
LED_indicator	91.35	98.88	94.72	98.69	99.83	98.50	87.86	14.32	24.53	67.00
PLCC_socket	97.83	99.73	97.18	99.90	99.99	99.75	99.07	81.15	74.26	92.30
VR_joystick	96.78	99.39	96.26	99.36	99.92	99.26	98.69	65.07	61.38	92.54
access_card	92.38	98.79	96.21	94.25	99.16	98.01	72.37	19.13	26.62	76.55
accurate_detection_switch	91.76	98.83	95.69	99.94	99.99	99.75	92.27	54.56	55.02	78.46
aircraft_model_head	99.98	100.00	99.85	99.98	100.00	99.75	98.74	48.08	55.45	93.28
angled_toggle_switch	97.02	99.46	98.15	99.92	99.99	99.50	88.00	21.64	29.03	64.48
audio_jack_socket	81.93	94.21	91.81	95.14	99.39	96.16	92.73	15.17	23.23	68.17
bag_buckle	99.69	99.96	98.94	100.00	100.00	100.00	99.70	80.60	74.18	98.48
ball_pin	99.51	99.94	99.00	99.96	100.00	99.75	99.34	67.01	63.48	97.00
balun_transformer	96.30	99.29	95.79	99.58	99.95	99.00	97.26	68.45	68.17	82.15
battery	81.51	97.02	94.36	88.46	98.38	96.59	88.86	23.16	30.30	64.43
battery_holder_connector	98.44	99.79	98.07	99.68	99.96	99.24	93.95	69.35	65.58	91.05
battery_socket_connector	89.31	98.01	93.83	96.96	99.62	96.84	96.39	57.29	59.41	86.11
bend_connector	92.23	98.86	93.75	99.62	99.95	99.24	94.72	48.97	49.32	85.84
blade_switch	99.40	99.92	99.15	99.96	100.00	99.75	97.21	50.22	54.07	88.49
blue_light_switch	86.27	97.31	92.97	91.48	98.66	96.59	93.46	33.84	41.82	78.00
bluetooth_module	99.65	99.96	99.10	100.00	100.00	100.00	97.77	73.44	68.14	89.14
boost_converter_module	92.65	98.46	94.93	98.71	99.84	98.25	96.02	66.37	64.06	77.53
bread_model	90.89	98.52	93.90	96.64	99.56	97.32	98.88	74.50	68.71	92.26
brooch_clasp_accessory	99.44	99.92	99.19	100.00	100.00	100.00	98.05	74.32	72.90	91.31
button_battery_holder	99.00	99.85	99.40	99.76	99.97	99.50	96.88	48.45	51.35	85.42
button_motor	98.58	99.78	99.24	98.80	99.83	99.24	99.47	77.75	73.52	95.86
button_switch	94.54	99.19	96.03	97.88	99.63	99.75	99.49	82.07	76.27	90.94
car_door_lock_switch	94.90	99.33	96.12	97.12	99.61	98.77	98.63	75.69	69.00	92.95
ceramic_fuse	93.16	99.08	95.03	98.58	99.80	99.50	92.37	41.46	47.63	82.77
ceramic_wave_filter	98.03	99.72	98.34	99.66	99.96	99.25	94.88	52.40	55.99	84.76

Continued on next page

Table A9: Per-category results of Meganomaly-B on Real-IAD Variety (continued).

Category	I-AUROC	I-AP	I-F1	O-AUROC	O-AP	O-F1	P-AUROC	P-AP	P-F1	P-AUPRO
charging_port	97.53	99.64	97.23	99.98	100.00	99.75	94.65	42.86	48.39	85.50
chip_inductor	94.86	99.25	97.35	99.82	99.98	99.24	93.45	46.94	49.06	76.07
circuit_breaker	99.44	99.93	98.80	100.00	100.00	100.00	98.90	67.47	65.51	95.26
circular_aviation_connector	86.15	95.77	89.38	97.07	99.49	98.75	93.87	42.46	52.00	78.23
common_mode_choke	89.18	97.69	92.15	91.94	98.93	95.63	95.96	48.60	51.60	78.97
common_mode_filter	97.78	99.69	97.70	99.34	99.92	98.27	94.94	49.83	51.47	80.00
connector	98.04	99.75	97.15	99.49	99.94	99.48	91.02	67.44	63.09	76.25
connector_housing_female	98.04	99.49	98.90	99.68	99.96	99.75	91.58	57.36	59.68	87.40
console_switch	99.87	99.98	99.60	100.00	100.00	100.00	86.57	29.58	34.97	81.17
crimp_st_cable_mount_box	96.71	99.33	97.22	97.62	99.61	98.75	99.36	71.40	69.14	94.89
dc_jack	93.43	98.75	95.81	99.78	99.97	99.50	90.38	53.91	48.72	84.86
dc_power_connector	98.80	99.85	98.36	100.00	100.00	100.00	94.61	41.33	42.90	90.08
detection_switch	93.74	98.41	95.76	98.76	99.84	98.75	94.77	49.22	50.99	79.97
duckbill_circuit_breaker	94.45	99.13	95.79	98.76	99.85	98.22	97.90	46.78	49.11	91.46
earphone_audio_unit	89.27	98.32	93.79	93.72	99.20	95.44	97.01	61.29	60.87	79.00
effect_transistor	96.39	99.15	96.00	98.06	99.75	98.25	99.37	81.23	76.05	94.42
electronic_watch_movement	78.17	96.67	94.08	82.02	97.41	94.29	97.25	53.42	53.34	79.45
ethernet_connector	98.18	99.70	97.33	99.40	99.91	99.43	97.67	60.11	60.18	87.43
ferrite_bead	96.43	99.42	97.07	97.34	99.63	98.03	98.94	67.91	66.09	92.12
ffc_connector_plug	98.04	99.60	97.72	98.92	99.86	99.01	98.76	48.28	53.84	93.80
flow_control_valve	93.24	98.82	95.81	99.17	99.89	98.75	98.99	63.98	60.69	94.26
flower_copper_shape	98.72	99.84	97.95	100.00	100.00	100.00	96.34	66.19	62.01	89.19
flower_velvet_fabric	97.25	99.65	97.08	99.48	99.94	99.24	93.26	67.29	64.69	79.84
fork_crimp_terminal	89.06	95.57	95.98	98.62	99.80	99.24	98.55	51.52	53.44	93.09
fuse_cover	91.51	98.37	94.46	96.11	99.49	98.26	95.52	58.83	57.02	86.28
fuse_holder	99.94	99.99	99.85	100.00	100.00	100.00	95.81	37.83	42.58	81.18
gear	99.47	99.89	99.80	100.00	100.00	100.00	99.20	80.33	76.73	95.80
gear_motor	86.91	97.20	97.36	89.67	98.36	97.55	88.76	19.00	27.77	82.72
green_ring_filter	91.81	97.58	91.08	99.32	99.92	99.25	95.50	39.81	45.52	78.08
hairdryer_switch	99.46	99.93	98.85	99.96	100.00	99.75	98.47	65.48	63.81	87.23
hall_effect_sensor	98.47	99.73	99.55	98.63	99.79	99.75	97.54	60.45	60.96	87.45
headphone_jack_female	99.94	99.99	99.90	100.00	100.00	100.00	95.28	68.84	70.00	87.53
headphone_jack_socket	88.93	98.47	93.96	92.14	99.01	95.15	97.00	59.28	59.36	85.55
hex_plug	96.10	99.53	96.05	99.90	99.99	99.50	95.42	62.69	59.46	83.57

Continued on next page

Table A9: Per-category results of Meganomaly-B on Real-IAD Variety (continued).

Category	I-AUROC	I-AP	I-F1	O-AUROC	O-AP	O-F1	P-AUROC	P-AP	P-F1	P-AUPRO
humidity_sensor	97.67	99.56	98.48	99.80	99.98	99.75	97.49	41.01	42.22	89.14
ingot_buckle	98.75	99.84	98.35	100.00	100.00	100.00	97.78	57.94	57.71	88.54
insect_metal_parts	90.44	97.50	96.71	99.37	99.92	98.49	96.04	31.45	37.23	85.70
inverter_connector	99.90	99.99	99.55	100.00	100.00	100.00	99.23	69.09	62.58	97.24
jam_jar_model	85.47	96.97	91.00	90.65	98.84	94.31	84.44	41.81	49.07	79.24
joystick_switch	99.97	100.00	99.90	100.00	100.00	100.00	99.52	61.43	55.55	98.61
kfc_push_key_switch	97.56	99.65	97.63	99.98	100.00	99.75	95.37	48.55	50.08	77.99
knob_cap	97.86	99.55	97.85	99.42	99.92	99.25	93.27	29.41	33.45	73.47
laser_diode	67.75	90.43	92.03	86.74	97.98	95.31	86.99	9.88	18.47	74.81
lattice_block_plug	84.02	96.07	93.61	98.15	99.76	98.00	97.38	32.76	42.82	85.69
lego_pin_connector_plate	99.52	99.92	99.90	99.96	99.99	99.75	98.41	64.56	64.91	90.48
lego_propeller	98.47	99.80	97.75	100.00	100.00	100.00	97.29	48.40	48.35	87.07
lego_reel	99.56	99.94	99.44	99.98	100.00	99.74	96.23	60.03	60.53	90.72
lego_technical_gear	98.37	99.75	97.75	100.00	100.00	100.00	98.84	69.22	66.84	94.35
lego_turbine	95.71	98.34	96.24	99.88	99.98	99.50	97.43	64.76	63.70	86.10
lighting_connector	87.10	96.74	90.66	84.87	97.90	94.51	95.50	48.23	51.29	68.89
lilypad_led	98.39	99.79	98.05	99.82	99.98	99.50	98.49	59.64	56.28	96.38
limit_switch	92.99	97.33	95.77	100.00	100.00	100.00	95.83	33.27	41.35	83.83
lithium_battery_plug	93.40	98.88	96.75	94.23	99.17	98.03	98.73	73.09	70.05	91.80
littel_fuse	98.57	99.82	98.06	100.00	100.00	100.00	96.39	59.46	58.94	89.42
little_cow_model	85.59	96.64	94.02	86.65	97.39	96.53	98.48	62.91	61.64	91.28
lock	97.70	99.61	98.45	100.00	100.00	100.00	91.84	44.50	44.13	73.69
long_zipper	97.36	99.64	96.29	98.45	99.81	97.77	91.55	27.48	35.06	80.42
meteor_hammer_arrowhead	91.79	98.07	95.75	99.98	100.00	99.75	97.80	54.56	51.78	88.53
miniature_laser_module	97.54	99.63	97.91	99.06	99.86	99.48	98.84	59.52	57.63	95.92
miniature_lifting_motor	88.77	98.37	94.51	91.96	98.82	97.31	98.30	80.37	73.22	66.49
miniature_motor	95.96	99.35	97.09	98.65	99.81	99.25	96.81	37.43	40.94	81.73
miniature_stepper_motor	96.72	99.47	97.72	95.46	99.26	97.79	91.96	47.43	48.29	67.29
mobile_charging_connector	98.88	99.85	99.00	99.78	99.97	99.75	98.19	77.01	72.79	89.15
model_steering_module	93.87	98.93	93.78	94.80	99.35	95.88	97.52	54.03	59.30	87.28
monitor_socket	99.49	99.93	98.92	99.76	99.97	99.49	98.56	69.08	62.26	90.16
motor_bracket	93.75	99.13	95.99	97.61	99.68	98.01	98.14	75.43	71.54	86.51
motor_gear_reducer	91.20	98.65	95.00	94.18	99.24	96.81	90.37	40.23	46.26	81.14
motor_plug	99.97	100.00	99.80	99.94	99.99	99.75	98.94	82.02	77.34	94.59

Continued on next page

Table A9: Per-category results of Meganomaly-B on Real-IAD Variety (continued).

Category	I-AUROC	I-AP	I-F1	O-AUROC	O-AP	O-F1	P-AUROC	P-AP	P-F1	P-AUPRO
mouse_socket	91.29	98.47	93.15	91.29	98.84	95.50	97.99	45.69	53.58	82.49
multi_function_switch	99.48	99.94	98.61	100.00	100.00	100.00	95.40	50.54	55.54	85.63
nylon_ball_head	97.02	99.59	97.72	98.82	99.84	99.00	96.68	63.39	61.48	88.21
optical_fiber_outlet	98.87	99.85	98.49	99.60	99.95	99.00	99.04	75.32	69.62	93.87
pencil_sharpener	96.66	99.44	96.94	99.82	99.98	99.49	98.15	53.66	50.75	89.73
pinboard_connector	96.15	99.43	98.01	98.88	99.86	98.49	97.66	46.07	52.36	94.34
pitch_connector	97.83	99.66	97.15	100.00	100.00	100.00	97.00	74.18	72.54	93.81
pneumatic_elbow	93.06	99.05	95.46	97.82	99.72	97.74	95.35	63.14	60.66	80.22
pot_core	95.90	99.40	97.32	99.48	99.93	99.50	91.36	44.89	47.49	55.43
potentiometer	99.44	99.89	98.57	100.00	100.00	100.00	99.08	59.32	57.78	96.09
power_bank_module	97.29	99.39	98.35	92.08	98.64	98.73	97.16	57.97	56.07	86.64
power_inductor	95.47	99.31	95.83	99.44	99.93	98.51	94.68	40.96	42.50	78.82
power_jack	79.68	96.90	94.06	87.60	98.26	95.67	90.00	4.60	10.21	62.93
power_strip_socket	91.69	97.50	90.37	98.46	99.80	98.51	98.80	67.87	65.58	92.55
pulse_transformer	87.27	97.10	96.26	98.81	99.84	98.71	94.48	56.67	56.70	86.14
purple_clay_pot	95.14	98.79	99.11	95.98	99.14	99.48	98.41	65.35	65.02	89.73
push_button_switch	95.75	99.14	98.58	100.00	100.00	100.00	97.88	46.25	47.96	87.09
push_in_terminal	97.95	99.76	97.25	99.72	99.97	99.25	98.74	51.28	52.80	94.56
recorder_switch	90.79	98.73	94.62	95.74	99.41	97.54	98.91	52.15	53.83	88.42
rectangular_connector_accessories	94.31	97.45	92.22	99.72	99.97	99.50	97.25	46.54	46.96	92.19
red_terminal	96.20	99.30	96.61	99.16	99.90	98.28	98.46	69.63	71.63	89.20
retaining_ring	96.09	99.15	95.40	99.84	99.98	99.49	84.05	47.21	44.03	64.11
rheostat	93.62	99.01	96.50	97.31	99.64	98.51	98.76	49.38	48.86	94.41
rotary_position_sensor	90.94	98.05	97.98	100.00	100.00	100.00	93.49	40.09	41.36	82.10
round_twist_switch	86.20	97.51	93.86	91.96	98.98	95.17	97.66	49.05	52.41	83.52
self_lock_switch	98.27	99.76	98.30	99.74	99.97	99.50	98.15	28.11	32.89	92.90
shelf_support_module	97.27	99.58	97.89	98.92	99.86	99.26	93.05	53.69	50.82	76.61
side_press_switch	99.26	99.91	98.48	100.00	100.00	100.00	98.51	70.22	68.55	89.41
side_release_buckle	95.44	99.41	96.50	99.58	99.95	99.00	97.10	43.45	47.49	94.28
silicon_cell_sensor	90.48	98.21	95.96	97.44	99.58	98.76	98.13	39.23	44.97	89.36
sim_card_reader	95.83	99.45	96.06	97.59	99.68	97.98	97.90	72.38	67.11	91.75
single_pole_potentiometer	88.53	98.08	93.31	96.88	99.61	97.52	94.96	18.54	30.94	71.19
single_switch	93.09	99.04	95.09	96.78	99.58	97.23	98.72	56.96	60.78	83.60
slide_switch	97.60	99.67	97.69	100.00	100.00	100.00	96.20	42.40	45.99	77.84

Continued on next page

Table A9: Per-category results of Meganomaly-B on Real-IAD Variety (continued).

Category	I-AUROC	I-AP	I-F1	O-AUROC	O-AP	O-F1	P-AUROC	P-AP	P-F1	P-AUPRO
slipper_model	95.94	99.39	97.35	98.00	99.73	98.76	98.95	63.12	65.19	95.42
small_leaf	93.81	98.88	95.15	97.86	99.73	97.76	97.71	43.59	48.57	89.39
smd_receiver_module	90.43	97.62	92.32	99.60	99.95	98.73	96.81	61.03	60.23	85.07
solderless_adapter	95.76	99.46	96.25	97.88	99.72	97.79	95.91	38.31	37.85	89.48
spherical_airstone	95.61	99.33	96.72	99.98	100.00	99.75	98.15	59.31	57.28	88.92
spring_antenna	95.14	99.12	95.60	98.16	99.77	98.25	97.54	60.61	59.14	90.10
square_terminal	96.09	99.23	97.77	97.15	99.50	99.26	87.47	56.35	57.27	82.38
steering_T_head	99.78	99.97	99.55	100.00	100.00	100.00	99.13	77.01	72.56	95.78
steering_wheel	93.85	99.16	96.45	95.98	99.46	97.56	98.80	79.05	72.12	90.09
suction_cup	94.41	98.89	95.50	99.84	99.98	99.25	97.98	65.58	63.30	86.74
telephone_spring_switch	98.75	99.84	98.31	99.84	99.98	99.75	99.29	80.15	72.21	95.47
tension_snap_release_clip	99.15	99.89	98.58	100.00	100.00	100.00	96.52	62.28	62.55	86.13
thumbtack	94.35	98.77	95.56	96.78	99.53	98.51	98.99	56.45	56.72	95.49
thyristor	99.95	99.99	99.95	100.00	100.00	100.00	94.43	33.40	38.33	89.79
toy_tire	96.96	99.53	96.81	99.58	99.95	99.00	97.23	66.03	62.35	83.34
traceless_hair_clip	99.24	99.90	98.26	99.78	99.97	99.25	98.73	72.61	68.14	86.33
travel_switch	93.16	99.08	95.41	98.38	99.77	98.74	86.85	21.01	28.18	62.76
travel_switch_green	99.55	99.94	99.20	100.00	100.00	100.00	97.64	49.84	49.39	93.06
tubular_key_switch	93.53	99.11	96.38	96.18	99.52	96.74	85.93	25.04	30.59	73.77
vacuum_switch	81.86	97.01	95.13	88.02	97.86	96.82	98.37	54.03	55.84	88.12
vehicle_harness_conductor	96.32	99.42	95.71	99.80	99.98	99.75	98.16	52.93	53.05	95.47
vertical_adjustable_resistor	95.86	98.76	95.02	98.84	99.84	99.00	97.82	54.72	56.84	90.71
vibration_motor	85.44	95.92	95.47	99.10	99.87	99.75	96.66	26.81	34.54	83.05
volume_potentiometer	86.92	96.42	92.42	92.44	98.81	97.28	96.50	69.15	69.46	78.72
wireless_receiver_module	96.47	99.50	97.46	98.16	99.75	98.50	91.00	46.08	46.79	83.05
Mean	94.55	98.92	96.58	97.75	99.67	98.71	95.75	53.86	54.50	85.39

Table A10: Per-category results of Meganomaly-B on ADNet. All values are percentages (%).

Source	Category	I-AUROC	I-AP	I-F1	P-AUROC	P-AP	P-F1	P-AUPRO
VisA	candle	99.05	99.09	95.52	99.19	41.37	46.49	92.03
	capsules	92.33	95.85	90.55	99.28	62.51	62.09	92.87
	cashew	94.96	97.47	93.00	98.37	57.48	57.67	95.53
	chewinggum	98.75	99.47	96.94	99.09	68.64	67.77	89.49
	fryum	98.52	99.29	95.61	96.45	41.80	48.91	89.57
	macaroni1	97.70	97.52	94.74	98.77	28.63	37.03	94.50
	macaroni2	93.39	94.06	87.32	98.61	16.67	28.15	95.79
	pcb1	99.65	99.68	97.98	99.48	78.49	72.46	95.00
	pcb2	97.71	98.31	94.00	98.42	34.47	41.61	89.86
	pcb3	96.44	96.45	92.08	98.77	29.66	32.90	91.66
	pcb4	99.88	99.88	98.51	98.54	50.10	51.03	93.38
	pipe_fryum	98.28	99.11	96.04	99.30	60.37	63.71	97.02
GoodsAD	cigarette_box	68.49	79.62	86.73	94.08	36.91	48.16	82.00
	drink_bottle	60.88	77.61	84.03	93.31	11.68	18.41	76.48
	drink_can	74.64	88.94	88.89	92.31	25.71	32.80	79.05
	food_bottle	70.91	86.95	86.36	95.42	28.20	36.11	82.70
	food_box	63.17	87.86	89.61	92.54	18.30	23.98	78.34
	food_package	65.22	81.36	82.67	94.61	18.17	26.23	79.38
KolektorSDD	KolektorSDD	95.88	95.55	95.05	84.64	9.58	19.56	68.49
FSSD-12	steel	100.00	100.00	100.00	88.84	57.74	57.01	61.32
KolektorSDD2	KolektorSDD2	95.88	96.80	91.18	98.75	67.02	63.70	95.95
MVTec-AD 2	can	50.06	55.25	72.87	74.41	0.07	0.74	25.18
	fabric	56.55	71.56	73.17	89.17	9.81	19.29	45.98
	fruit_jelly	91.75	97.35	91.20	95.26	37.89	46.01	70.75
	rice	72.14	86.47	82.95	90.02	16.71	28.98	62.39
	sheet_metal	83.61	95.45	90.45	74.95	9.03	19.50	35.84
	vial	90.29	96.35	92.31	93.45	32.89	36.67	90.39
	wallplugs	38.56	56.41	75.00	84.58	8.98	18.00	38.26
	walnuts	91.61	95.47	87.95	96.20	59.78	62.36	77.53
WMH	brain_wmh	61.93	57.65	69.75	96.18	8.98	17.59	74.89

Continued on next page

Table A10: Per-category results of Meganomaly-B on ADNet (continued).

Source	Category	I-AUROC	I-AP	I-F1	P-AUROC	P-AP	P-F1	P-AUPRO
Liver_AD	liver_pathology	68.96	64.33	72.99	97.49	16.25	26.09	93.75
BraTS2021	brain_tumor_brats2021	78.47	74.09	75.93	94.99	39.50	44.46	73.33
MPDD	bracket_black	87.37	92.70	82.98	97.09	16.31	25.87	91.86
	bracket_brown	94.34	96.65	94.44	98.61	43.12	43.05	95.25
	bracket_white	95.11	95.92	88.14	99.11	12.09	22.43	95.02
	connector	100.00	100.00	100.00	99.02	66.29	62.54	96.79
	metal_plate	100.00	100.00	100.00	97.26	79.55	76.81	91.77
	tubes	95.38	98.32	94.66	99.19	78.99	73.98	97.05
AeBAD	AeBAD_S	93.47	98.15	94.66	95.30	19.27	25.39	90.87
Real-IAD	audiojack	91.09	97.31	93.54	95.98	35.53	44.16	81.66
	bottle_cap	95.64	98.92	94.36	99.56	41.41	42.07	97.66
	button_battery	93.09	97.79	94.97	98.46	55.10	56.20	90.99
	end_cap	89.49	97.10	92.24	97.98	22.51	31.04	93.48
	eraser	95.16	98.63	94.82	99.44	42.81	45.79	96.43
	fire_hood	85.48	95.95	90.82	98.52	38.10	44.94	90.93
	mint	78.43	91.75	86.62	95.63	21.48	32.07	76.72
	mounts	96.95	99.04	94.74	99.16	39.51	45.20	94.00
	pcb	91.35	97.71	92.33	98.72	46.83	51.31	92.31
	phone_battery	96.95	99.21	95.94	98.99	40.19	43.28	95.11
	plastic_nut	91.69	97.60	93.23	99.07	33.70	37.45	96.11
	plastic_plug	92.87	98.26	92.74	98.37	31.22	38.94	93.67
	porcelain_doll	95.73	98.61	94.28	98.88	37.54	42.54	95.09
	regulator	77.52	93.68	90.02	97.13	28.45	38.44	88.83
	rolled_strip_base	99.53	99.84	99.17	99.77	43.90	51.55	99.15
	sim_card_set	97.28	98.57	97.22	98.66	50.70	52.75	93.95
	switch	96.93	99.04	94.93	98.32	52.90	57.82	94.45
	tape	98.84	99.71	97.51	99.26	38.05	47.14	97.13
	terminalblock	99.25	99.76	98.32	99.79	49.68	51.77	98.81
	toothbrush	91.52	97.18	91.18	97.18	41.15	46.72	90.77
	toy	86.05	95.93	91.61	93.85	19.34	28.46	86.47
	toy_brick	79.81	94.02	89.49	98.40	40.30	46.87	89.73
	transistor1	97.28	99.12	94.96	98.87	45.76	47.22	95.82

Continued on next page

Table A10: Per-category results of Meganomaly-B on ADNet (continued).

Source	Category	I-AUROC	I-AP	I-F1	P-AUROC	P-AP	P-F1	P-AUPRO
	u_block	93.84	98.39	93.79	99.16	43.58	49.80	95.24
	usb	93.56	98.26	93.58	98.94	39.69	44.87	94.27
	usb_adaptor	94.82	98.61	94.12	98.56	25.04	35.03	90.87
	vcpill	92.48	98.14	92.25	98.90	57.43	60.77	93.61
	wooden_beads	88.65	96.78	91.93	98.59	45.51	48.75	93.35
	woodstick	80.76	94.79	89.91	97.30	43.61	51.56	86.35
	zipper	99.86	99.97	99.50	99.19	61.74	63.90	97.47
DAGM	DAGM_Class1	99.76	99.74	99.01	88.16	53.64	54.85	79.46
	DAGM_Class2	100.00	100.00	100.00	99.71	68.95	66.57	99.21
	DAGM_Class3	99.92	99.92	99.00	97.39	70.51	68.92	95.18
	DAGM_Class4	100.00	100.00	100.00	98.51	77.90	73.13	95.87
	DAGM_Class5	100.00	100.00	100.00	99.12	83.59	77.16	97.41
	DAGM_Class6	100.00	100.00	100.00	98.59	78.28	75.60	95.91
	DAGM_Class7	100.00	100.00	100.00	97.59	83.25	78.37	96.14
	DAGM_Class8	97.32	97.97	92.63	97.61	59.00	61.73	95.65
	DAGM_Class9	99.00	98.65	98.00	99.77	62.43	63.09	99.26
	DAGM_Class10	100.00	100.00	100.00	99.51	72.60	68.96	98.79
BH-WATERTANKS	REGION_1	60.18	60.41	70.42	85.19	5.90	11.97	55.07
	REGION_2	63.80	58.17	70.16	85.41	5.14	11.10	56.05
	REGION_3	64.56	64.01	70.42	86.38	7.09	14.19	60.52
	REGION_4	52.84	50.74	68.29	84.96	5.28	11.20	55.90
	REGION_5	67.52	63.08	73.21	86.80	6.33	12.96	59.80
	REGION_6	51.89	49.74	67.35	83.83	4.79	10.48	52.96
CID	insulator	96.05	98.92	94.07	98.72	63.94	68.01	86.20
Pavement-Defect-Datasets	ABCRACK500	94.39	94.02	90.55	95.09	55.96	58.91	83.21
	ABGF	99.40	99.68	98.02	92.10	72.16	68.15	77.43
	gapsab	98.92	99.16	95.65	92.95	56.27	61.48	80.23
Real-IAD-D3	audio_jack_socket	98.15	99.79	98.04	95.59	28.02	36.98	77.59
	common_mode_filter	99.00	99.87	99.25	91.81	19.12	29.21	61.08
	connector_housing_female	100.00	100.00	100.00	96.63	57.81	58.25	81.32
	crimp_st_cable_mount_box	100.00	100.00	100.00	91.31	15.36	28.74	60.82
	dc_power_connector	97.24	99.67	96.77	95.68	36.29	44.04	79.76

Continued on next page

Table A10: Per-category results of Meganomaly-B on ADNet (continued).

Source	Category	I-AUROC	I-AP	I-F1	P-AUROC	P-AP	P-F1	P-AUPRO
	ethernet_connector	98.83	99.78	99.34	98.89	41.10	45.92	96.03
	ferrite_bead	100.00	100.00	100.00	97.26	21.70	29.30	87.00
	fork_crimp_terminal	98.77	99.83	97.74	98.74	43.78	50.70	92.18
	fuse_holder	98.99	99.83	98.00	99.34	36.25	42.67	97.96
	headphone_jack_socket	99.97	100.00	99.80	95.12	10.84	15.62	81.60
	humidity_sensor	91.48	98.95	94.79	93.78	31.11	40.62	78.75
	knob_cap	99.97	100.00	99.67	99.01	71.25	69.37	96.10
	lattice_block_plug	95.88	99.45	97.52	92.42	10.32	17.94	76.82
	lego_pin_connector_plate	97.87	99.72	98.51	99.29	76.99	74.11	94.10
	lego_propeller	100.00	100.00	100.00	83.60	0.57	1.34	47.37
	limit_switch	98.68	99.83	98.26	97.52	29.97	36.42	94.72
	miniature_lifting_motor	95.28	98.71	96.04	91.44	15.65	27.13	66.82
	power_jack	97.89	99.60	98.36	88.41	3.86	9.49	54.22
	purple_clay_pot	93.34	98.95	96.37	99.57	75.35	69.91	95.14
	telephone_spring_switch	91.22	99.08	96.05	97.62	47.96	51.20	88.82
3CAD	Aluminum_Camera_Cover	90.76	98.47	96.20	88.98	38.03	42.52	81.08
	Aluminum_Ipad	93.74	97.47	93.86	97.32	22.97	33.77	87.37
	Aluminum_Middle_Frame	85.53	95.29	91.06	95.48	13.77	23.35	76.77
	Aluminum_New_Ipad	74.90	91.83	90.16	94.38	17.87	28.46	73.93
	Aluminum_New_Middle_Frame	67.38	81.21	83.88	90.42	6.97	14.09	62.60
	Aluminum_Pc	68.97	94.91	94.46	82.86	4.38	10.00	58.41
	Copper_Stator	83.70	87.82	85.97	96.12	17.51	26.81	84.17
	Iron_Stator	69.05	87.73	87.48	89.24	14.95	23.56	59.59
HRSID	ship	87.05	94.50	90.09	98.66	16.96	28.02	94.00
pill	ginseng	100.00	100.00	100.00	99.45	65.23	67.53	98.28
	magnesium	99.87	99.98	99.50	99.46	74.45	72.10	97.74
	mint	100.00	100.00	100.00	81.26	49.53	51.04	77.76
MAD-real	Bear	71.67	86.61	94.12	99.59	15.06	27.49	98.64
	Bird	72.73	89.29	89.80	89.80	14.03	24.83	75.41
	Elephant	73.15	89.16	87.18	86.18	9.48	22.23	66.92
	Parrot	61.59	88.80	88.46	60.28	1.07	2.67	48.66
	Pig	72.27	87.67	85.00	97.05	24.56	28.68	87.42
	Puppy	93.33	98.00	95.24	99.26	33.14	39.29	95.90

Continued on next page

Table A10: Per-category results of Meganomaly-B on ADNet (continued).

Source	Category	I-AUROC	I-AP	I-F1	P-AUROC	P-AP	P-F1	P-AUPRO
	Scorpion	31.88	78.18	88.46	70.79	3.03	7.04	29.86
	Turtle	100.00	100.00	100.00	99.43	37.41	48.94	97.85
	Unicorn	47.62	77.66	89.36	83.06	1.21	3.18	51.36
	Whale	96.35	99.32	96.87	99.48	38.14	45.87	97.46
BH-POOLS	REGION_1	74.26	67.95	75.97	82.75	13.79	21.57	60.10
	REGION_2	84.64	79.93	79.21	81.88	11.96	20.78	59.04
	REGION_3	76.02	70.22	74.40	83.08	13.28	21.98	58.65
	REGION_4	75.47	71.17	74.40	81.90	11.83	19.34	57.53
	REGION_5	73.57	69.69	75.10	79.39	13.21	20.85	52.30
	REGION_6	75.49	72.22	73.45	80.46	15.12	22.11	67.11
	REGION_7	75.16	71.98	72.73	74.36	9.04	16.92	58.58
	REGION_8	72.42	66.92	75.38	84.22	11.49	18.84	60.25
DeepPCB	DeepPCB_group00041	87.26	96.39	93.46	95.12	44.07	46.36	83.33
	DeepPCB_group12100	91.85	98.25	96.61	93.50	38.34	41.40	79.00
	DeepPCB_group12300	92.14	99.11	96.97	92.01	36.67	39.84	75.18
	DeepPCB_group13000	93.36	98.41	96.15	95.45	47.26	48.82	83.78
	DeepPCB_group20085	83.88	93.36	90.57	93.50	30.93	36.11	77.93
	DeepPCB_group44000	95.70	99.45	99.50	95.84	50.75	55.21	85.12
	DeepPCB_group50600	100.00	100.00	100.00	96.74	54.58	55.06	89.26
	DeepPCB_group77000	90.91	97.79	99.01	97.74	56.38	57.27	92.06
	DeepPCB_group90100	72.30	95.59	97.37	90.82	29.01	34.54	69.84
	DeepPCB_group92000	100.00	100.00	100.00	98.07	72.96	68.12	92.88
LiTS	liver_tumor	68.24	63.88	72.09	90.12	1.51	3.76	56.09
MSLUB	ms_lesion	83.05	82.22	78.30	95.09	9.09	16.81	70.32
Datasheet_VIADUCT	00 shredded corn rough	76.90	97.58	96.22	83.72	26.48	31.87	72.21
	01 shredded corn medium	94.84	98.74	93.95	91.47	35.01	39.47	84.83
	02 shredded corn fine	93.44	99.17	96.89	93.99	37.71	41.64	87.40
	03 3-pole socket housing	90.41	98.92	95.05	93.14	32.29	38.81	78.80
	04 battery tray	73.25	93.51	88.89	96.36	32.99	40.82	81.83
	05 cable end sleeve	86.47	92.50	84.62	97.68	11.56	21.54	92.74
	06 coaxial t-adapter	84.44	91.60	82.61	97.16	69.54	67.00	89.76
	07 d-sub connector	86.67	95.17	85.71	98.72	8.57	19.97	96.03

Continued on next page

Table A10: Per-category results of Meganomaly-B on ADNet (continued).

Source	Category	I-AUROC	I-AP	I-F1	P-AUROC	P-AP	P-F1	P-AUPRO
	08 ethernet connector	80.94	91.68	93.67	95.79	17.88	25.22	88.44
	09 joystick	60.78	89.96	91.07	98.76	66.91	63.13	91.97
	10 PCB	77.73	95.94	93.22	98.75	18.59	26.45	95.84
	11 ring cable lug	89.92	96.74	91.43	95.56	28.28	32.52	89.04
	12 rotary encoder	76.29	93.18	87.88	97.58	25.01	34.98	92.00
	13 socket housing	86.77	97.61	94.57	91.77	38.69	45.25	84.97
	14 terminal block A	74.98	94.96	92.39	97.32	41.07	45.98	83.04
	15 terminal block B	82.67	96.33	94.49	96.20	42.73	46.28	88.37
	16 vibration sensor	83.33	95.36	92.06	94.92	14.15	24.99	82.81
	17 cherry	81.82	91.20	89.26	99.22	34.60	39.22	95.61
	18 raspberry	94.59	98.37	95.29	98.78	60.26	57.73	93.13
	19 strawberry	91.83	97.89	94.98	94.80	40.71	50.35	81.59
	20 tea bag	94.75	99.02	94.47	99.49	53.68	58.49	97.94
	21 cylinder screw	96.75	97.57	91.43	99.44	61.60	59.36	98.40
	22 device box	75.27	95.32	92.00	99.14	16.05	28.67	93.97
	23 pipe clamp	90.95	97.65	93.10	88.19	45.63	53.99	87.42
	24 pan screw	82.37	96.05	93.84	99.28	13.53	21.93	96.95
	25 reinforcing sleeve	89.29	95.40	95.45	98.59	30.60	36.11	95.49
	26 hose screw fitting	94.40	98.58	93.10	98.14	37.67	41.01	94.12
	27 L-fitting	83.65	95.01	88.89	98.50	31.12	39.25	91.91
	28 key	95.96	98.44	97.56	98.55	70.56	64.61	95.14
	29 threaded fitting	50.85	87.71	92.31	98.28	12.52	19.95	93.90
	30 valve handle blue	99.48	99.83	97.96	99.04	24.06	34.72	96.52
	31 valve handle red	86.26	96.34	90.91	98.92	21.99	31.13	96.67
	32 bone pliers	86.51	94.93	89.17	99.66	39.94	41.68	97.63
	33 drill	68.92	94.15	92.21	98.99	18.96	28.64	93.85
	34 oblong pill	100.00	100.00	100.00	99.45	46.16	50.25	98.59
	35 pink tablet	85.18	98.06	96.55	94.27	40.23	53.00	87.91
	36 redon needle	99.18	99.75	97.96	99.65	31.95	39.14	98.38
	37 retractor	94.40	98.29	92.72	99.21	43.60	47.61	95.37
	38 round pill	97.55	99.79	98.40	97.54	24.68	31.85	95.67
	39 self-tapping bolt	98.80	99.84	98.66	98.76	59.00	57.90	90.50
	40 surgical mask	54.69	93.04	94.66	96.56	2.90	9.33	85.91
	41 white tablet	69.32	97.53	96.49	98.27	34.21	40.92	94.96
	42 aluminium plate	100.00	100.00	100.00	97.34	23.71	31.96	93.46

Continued on next page

Table A10: Per-category results of Meganomaly-B on ADNet (continued).

Source	Category	I-AUROC	I-AP	I-F1	P-AUROC	P-AP	P-F1	P-AUPRO
	43 paperclip	98.20	99.61	97.30	98.25	35.57	46.04	94.00
	44 tack	92.25	98.77	94.44	99.10	29.48	42.78	97.29
	45 damper large	93.00	98.58	94.34	98.69	81.95	74.15	88.34
	46 damper small	91.03	98.48	93.55	99.67	60.66	64.28	97.30
	47 mains tester	67.08	89.53	90.91	96.80	0.97	4.74	88.31
	48 saw blade	70.42	89.65	89.55	98.68	10.26	19.73	94.65
HAD	UTM_N	83.69	93.90	91.09	94.36	33.04	38.20	72.09
DTD-Synthetic	Blotchy_099	100.00	100.00	100.00	99.54	71.68	71.88	98.80
	Fibrous_183	100.00	100.00	100.00	99.52	68.70	70.54	98.55
	Marbled_078	99.75	99.94	98.75	99.64	77.38	75.69	98.71
	Matted_069	100.00	100.00	100.00	99.66	75.59	72.05	86.89
	Mesh_114	98.19	99.31	96.82	98.80	69.46	67.61	96.37
	Perforated_037	100.00	100.00	100.00	99.40	68.88	67.57	98.66
	Stratified_154	99.31	99.83	97.56	99.53	66.41	65.18	98.85
	Woven_001	99.90	99.96	99.29	99.62	64.99	66.52	97.58
	Woven_068	100.00	100.00	100.00	99.44	73.56	70.62	98.49
	Woven_104	100.00	100.00	100.00	99.57	76.43	72.04	98.72
	Woven_125	100.00	100.00	100.00	99.67	79.58	74.40	98.65
	Woven_127	98.75	99.16	98.73	95.71	65.16	67.29	95.35
MANTA	block_inductor	90.78	96.30	90.84	96.66	63.84	62.42	86.09
	button	93.25	95.31	91.75	98.74	44.59	52.89	90.59
	capsule	97.14	99.44	96.52	86.25	66.23	64.18	76.35
	coated_tablet	97.94	99.01	95.81	99.47	81.11	79.91	95.92
	coffee_beans	66.27	91.12	91.79	81.99	56.24	60.01	61.07
	copper_standoff	96.68	98.35	93.79	97.92	64.83	63.68	90.05
	embossed_tablet	97.25	98.36	95.94	98.06	60.72	60.80	92.78
	flat_nut	93.37	94.75	89.66	98.12	58.63	57.37	91.94
	gear	95.37	98.14	93.54	96.86	49.54	52.04	87.67
	goji_berries	84.87	96.09	89.62	92.94	61.42	58.70	78.73
	led	98.62	99.16	97.30	98.67	54.08	59.39	94.94
	led_pad	98.55	99.43	96.67	98.14	65.62	63.35	92.14
	lettered_tablet	97.16	98.51	94.79	98.52	67.54	64.82	94.66
	long_button	98.14	99.10	95.80	96.42	41.24	45.50	85.40

Continued on next page

Table A10: Per-category results of Meganomaly-B on ADNet (continued).

Source	Category	I-AUROC	I-AP	I-F1	P-AUROC	P-AP	P-F1	P-AUPRO
	maize	69.93	93.82	93.40	81.58	44.27	50.10	58.41
	nut	94.06	91.86	84.85	98.76	44.62	48.31	95.56
	nut_cap	84.93	85.97	80.91	96.85	32.81	38.48	88.62
	oblong_tablet	93.60	97.13	92.18	97.13	52.89	56.52	89.42
	paddy	91.80	98.71	95.07	74.74	30.36	35.17	64.18
	pink_tablet	97.12	99.12	94.75	98.66	65.16	66.02	92.81
	pistachios	77.19	90.32	89.54	76.71	26.10	32.86	59.91
	power_inductor	95.45	97.53	94.01	95.85	50.90	56.04	83.12
	red_tablet	90.64	96.35	91.84	75.41	33.97	43.83	76.23
	red_washer	98.49	99.45	96.09	98.08	46.25	48.65	94.29
	round_button_cap	98.44	99.41	96.59	98.43	50.42	54.28	93.23
	screw	93.85	97.54	93.06	96.13	49.57	54.27	88.11
	short_button	94.61	98.42	92.83	97.49	60.99	62.25	91.90
	soybean	85.34	96.95	94.69	84.24	56.34	59.85	64.74
	square_button_cap	99.36	99.81	98.31	98.22	66.10	64.83	92.22
	terminal	95.70	98.83	95.24	97.57	56.68	57.37	91.66
	thin_resistor	97.35	98.33	95.48	97.78	58.23	58.06	91.65
	type_c	98.57	99.35	95.89	97.18	40.98	46.00	86.61
	wafer_resistor	96.93	98.40	94.27	98.60	72.28	67.18	93.15
	wheat	90.96	98.49	95.63	91.15	52.10	52.68	75.88
	white_tablet	98.56	99.49	97.75	96.16	57.42	58.02	91.49
	wire_cap	96.17	98.91	94.84	97.44	39.46	46.21	91.40
	yellow_green_washer	95.01	98.21	93.47	92.30	36.83	43.62	88.52
	yellow_tablet	99.27	99.62	97.32	98.71	65.64	64.96	95.28
MIAD	catenary_dropper	91.30	96.78	91.99	90.93	18.89	29.53	82.35
	electrical_insulator	59.89	60.39	68.33	97.92	8.22	17.21	92.04
	metal_welding	96.04	97.99	92.94	96.87	19.52	29.26	84.95
	nut_and_bolt	69.69	86.68	85.96	94.59	14.48	21.95	82.19
	photovoltaic_module	92.21	97.19	93.06	98.34	36.96	43.48	87.44
	wind_turbine	98.74	98.83	94.58	99.56	19.49	30.57	92.98
	witness_mark	64.21	58.26	73.15	82.22	4.28	9.64	54.94
Magnetic-tile	Magnetic-tile	89.29	96.97	91.98	80.17	35.01	38.88	77.76
MAD-sim	01Gorilla	73.13	96.22	94.74	95.41	16.96	26.27	85.51

Continued on next page

Table A10: Per-category results of Meganomaly-B on ADNet (continued).

Source	Category	I-AUROC	I-AP	I-F1	P-AUROC	P-AP	P-F1	P-AUPRO
	02Unicorn	80.26	97.09	94.97	91.26	10.41	18.41	80.12
	03Mallard	83.76	97.36	93.26	86.51	12.39	21.61	70.46
	04Turtle	77.40	96.34	93.52	93.76	19.74	31.57	82.42
	05Whale	80.08	97.46	95.32	93.57	20.04	33.35	88.99
	06Bird	74.41	94.83	94.79	92.93	10.41	18.34	83.56
	07Owl	76.91	96.18	94.15	93.32	12.21	21.97	84.14
	08Sabertooth	69.37	94.76	94.25	91.73	5.69	10.30	80.45
	09Swan	69.77	95.25	94.50	93.98	12.31	20.93	87.05
	10Sheep	76.65	96.90	94.17	95.29	15.68	24.61	90.63
	11Pig	69.32	96.20	95.16	97.28	22.58	33.13	90.06
	12Zalika	74.29	96.32	94.85	90.03	12.53	19.43	77.28
	13Pheonix	53.17	91.26	95.31	89.05	6.79	11.87	80.97
	14Elephant	76.11	96.90	94.98	74.78	10.62	22.80	75.82
	15Parrot	68.26	93.36	93.30	88.38	10.73	19.40	76.72
	16Cat	62.23	94.62	95.33	95.59	13.42	24.26	91.23
	17Scorpion	85.87	98.02	95.73	93.16	12.79	20.86	87.41
	18Obesobeso	87.63	98.69	95.60	96.24	24.84	34.93	92.67
	19Bear	74.38	96.57	95.18	93.25	18.53	26.80	84.26
	20Puppy	60.59	93.90	94.38	91.61	11.24	19.73	80.54
MVTec-3D	bagel	81.52	94.11	89.12	99.21	54.74	55.18	96.03
	cable_gland	98.53	99.56	97.75	99.65	56.05	57.37	98.88
	carrot	93.49	98.33	93.04	99.54	45.33	47.89	98.28
	cookie	91.64	97.96	92.23	98.96	63.40	61.25	95.65
	dowel	94.12	98.06	92.79	99.58	52.81	52.86	98.05
	foam	87.33	95.66	88.20	94.31	35.28	43.02	83.38
	peach	94.47	97.64	94.34	99.66	57.21	57.29	98.66
	potato	78.77	90.89	86.83	99.39	34.97	38.95	97.51
	rope	99.73	99.86	98.53	99.58	57.11	58.65	98.53
	tire	89.10	96.51	90.43	99.12	37.46	43.43	95.97
MVTec loco	breakfast_box	85.51	96.04	90.57	88.27	56.47	55.16	76.60
	juice_bottle	96.39	99.09	96.20	89.05	48.69	51.87	86.21
	pushpins	83.29	94.21	88.02	56.52	4.93	10.88	64.21
	screw_bag	71.95	91.32	87.08	69.45	11.17	13.64	59.35

Continued on next page

Table A10: Per-category results of Meganomaly-B on ADNet (continued).

Source	Category	I-AUROC	I-AP	I-F1	P-AUROC	P-AP	P-F1	P-AUPRO
	splicing_connectors	89.62	97.19	90.32	68.76	24.71	25.90	66.44
AITEX	AITEX	89.96	87.65	85.85	92.94	33.49	48.44	76.54
Hyper-Kvasir	polyp_detection	90.99	85.98	88.57	83.51	24.85	35.39	51.80
wood-anomaly-detection	wood	84.23	84.32	78.10	88.22	24.44	30.42	66.31
PIAD-Sim	Amphora_IL	98.70	99.49	96.48	97.75	54.75	55.02	81.64
	Axletree_CL	93.93	98.83	95.38	98.60	70.42	63.63	89.24
	Box_CL	98.26	99.51	97.35	98.77	40.14	44.29	89.38
	Can_CL	99.21	99.85	98.34	99.01	53.57	54.10	87.77
	Chain_CL	91.20	98.57	93.61	98.59	27.44	35.23	94.56
	Gear_CL	99.67	99.93	98.68	96.12	53.25	53.18	83.19
	Keyring_CL	98.56	99.83	97.97	98.74	46.01	50.37	90.53
	Motor_CL	91.10	98.29	94.44	93.81	31.63	38.43	74.80
	Parts_CL	84.52	97.45	93.87	98.31	33.51	39.89	91.73
	Picker_CL	85.57	97.57	94.26	98.03	29.73	36.02	87.89
	Section_CL	99.55	99.92	99.14	98.68	39.20	42.94	93.34
	Shaft_CL	99.59	99.91	98.96	99.40	49.30	54.87	91.67
	Spray_can_CL	99.98	100.00	99.82	98.75	42.71	44.68	89.47
	Spring_CL	91.52	98.52	94.25	96.54	50.97	54.19	89.49
	Sprockets_CL	87.91	98.04	93.07	94.19	25.80	31.88	76.35
	Teapot_IL	94.70	99.25	96.37	97.44	31.35	37.67	84.28
BTAD	btad_01	99.53	99.59	97.03	97.33	57.51	57.02	79.86
	btad_02	85.40	93.94	86.24	96.39	56.55	59.97	65.28
	btad_03	99.84	99.46	98.41	99.31	66.19	61.67	97.27
MulSen_AD	button_cell	100.00	100.00	100.00	99.74	47.47	48.50	99.20
	capsule	99.09	99.83	97.62	99.39	55.19	58.72	95.55
	cotton	100.00	100.00	100.00	99.56	71.13	67.78	98.92
	cube	100.00	100.00	100.00	99.41	53.10	56.94	93.99
	flat_pad	92.00	97.26	93.55	99.33	30.31	37.02	98.04
	light	98.61	98.66	96.00	99.76	40.38	49.71	98.56
	nut	99.47	99.77	98.31	99.41	21.84	28.77	98.08
	piggy	99.71	99.89	98.31	98.50	35.01	41.45	94.44
	plastic_cylinder	98.82	99.38	96.97	99.35	38.33	45.65	98.15

Continued on next page

Table A10: Per-category results of Meganomaly-B on ADNet (continued).

Source	Category	I-AUROC	I-AP	I-F1	P-AUROC	P-AP	P-F1	P-AUPRO
	screen	100.00	100.00	100.00	97.01	38.03	41.30	92.91
	screw	100.00	100.00	100.00	99.08	21.36	27.55	97.75
	solar_panel	92.50	90.86	96.00	99.13	39.73	40.52	98.10
	spring_pad	98.26	99.27	95.83	99.72	22.13	28.45	99.03
	toothbrush	99.58	99.76	97.56	99.37	11.41	19.97	98.08
	zipper	100.00	100.00	100.00	97.81	20.20	26.80	94.56
AutoVI	engine_wiring	86.46	92.64	89.46	88.42	29.28	39.44	73.99
	pipe_clip	79.74	87.16	89.19	94.15	21.05	30.17	84.22
	pipe_staple	83.63	89.11	92.02	87.78	16.38	27.65	65.26
	tank_screw	54.51	61.56	75.50	95.64	5.71	12.16	82.52
	underbody_pipes	99.62	99.88	99.04	98.38	51.84	52.85	96.87
	underbody_screw	100.00	100.00	100.00	99.94	57.13	59.42	99.81
RAD-AD	Robust	97.38	99.22	98.88	92.90	37.41	42.15	86.89
ATLAS	stroke_lesion	80.82	83.80	75.96	96.21	16.64	25.53	80.30
MVTec-AD	bottle	100.00	100.00	100.00	98.87	81.52	79.61	96.78
	cable	97.11	99.13	95.19	97.68	62.20	63.50	91.31
	capsule	99.93	99.98	99.54	98.89	57.17	55.53	97.66
	carpet	100.00	100.00	100.00	99.45	75.54	68.32	97.61
	grid	100.00	100.00	100.00	99.32	49.15	54.46	97.02
	hazelnut	99.84	99.90	99.29	99.19	69.52	70.30	96.72
	leather	100.00	100.00	100.00	99.41	54.06	54.75	98.73
	metal_nut	100.00	100.00	100.00	96.89	72.62	77.89	94.86
	pill	99.43	99.88	98.19	97.40	59.35	61.85	97.69
	screw	97.73	99.31	96.27	99.47	52.67	51.53	97.57
	tile	100.00	100.00	100.00	96.83	68.35	71.04	92.21
	toothbrush	100.00	100.00	100.00	98.92	52.90	63.15	94.57
	transistor	99.91	99.94	98.77	94.90	60.24	60.92	87.92
	wood	100.00	100.00	100.00	95.98	64.39	61.08	95.28
	zipper	99.97	99.99	99.58	98.35	69.29	67.60	95.53
MSD-Seg	AI	100.00	100.00	100.00	93.98	70.90	67.55	83.96
	MT	93.26	98.95	97.24	73.74	59.79	53.14	57.99
	Rail	99.47	99.85	99.24	96.94	56.69	57.60	84.89

Continued on next page

Table A10: Per-category results of Meganomaly-B on ADNet (continued).

Source	Category	I-AUROC	I-AP	I-F1	P-AUROC	P-AP	P-F1	P-AUPRO
	Steel	100.00	100.00	100.00	87.80	51.98	51.90	80.19
	leather	100.00	100.00	100.00	88.60	52.92	49.90	67.74
	tile	100.00	100.00	100.00	88.53	66.05	63.14	57.24
Brain_AD	brain_tumor	92.90	93.59	85.71	98.22	69.29	64.97	85.83
PIAD-Real	01Valve_CL	97.10	99.34	97.38	91.32	28.05	39.43	91.95
	02Tube_CL	100.00	100.00	100.00	92.95	47.62	57.66	83.35
	03Cup_CL	99.93	99.99	99.70	99.62	63.31	64.49	98.32
	04USB_CL	78.29	93.60	91.40	98.67	36.63	39.86	92.84
	05Joint_CL	77.55	90.94	90.48	97.39	13.88	20.21	90.97
	06PaperCup_CL	99.33	99.84	98.80	99.32	68.44	60.78	98.43
	07Lighter_CL	100.00	100.00	100.00	99.50	77.12	74.35	98.45
	08Cube_CL	100.00	100.00	100.00	99.80	89.57	80.67	99.37
	09Lamp_CL	100.00	100.00	100.00	92.72	24.84	31.63	65.66
	10Bolt_CL	100.00	100.00	100.00	99.83	32.01	43.27	99.38
	11Filter_IL	100.00	100.00	100.00	99.92	54.95	57.05	99.74
	12Wand_IL	100.00	100.00	100.00	99.93	72.79	69.53	99.77
	13Wheel_IL	78.07	88.43	86.03	89.70	8.26	12.57	88.93
	14Bearing_IL	98.62	98.73	98.92	99.45	65.66	66.70	98.48
Sliver	liver_detection	90.22	89.95	83.58	82.51	12.28	20.56	53.20
WFDD	grey_cloth	99.95	99.97	99.16	98.91	63.81	62.58	90.07
	grid_cloth	98.11	97.09	93.69	98.91	40.94	44.01	92.51
	pink_flower	96.39	96.46	91.18	99.73	87.96	82.06	91.46
	yellow_cloth	99.01	99.15	96.34	97.15	33.40	41.71	91.82
Mean		**89.10**	**94.78**	**93.22**	**94.86**	**39.66**	**43.91**	**85.66**

Table A11: Per-category results of Meganomaly-B on Real-IAD. All values are percentages (%).

Category	I-AUROC	I-AP	I-F1	O-AUROC	O-AP	O-F1	P-AUROC	P-AP	P-F1	P-AUPRO
audiojack	91.93	87.61	78.14	95.09	97.18	94.23	99.46	49.85	51.92	96.67
bottle_cap	97.91	97.55	92.53	98.48	99.32	95.15	99.78	43.68	42.90	98.88
button_battery	93.58	93.59	88.30	95.86	96.36	95.60	99.09	40.65	53.90	94.97
end_cap	90.97	91.59	86.10	94.96	97.46	92.07	99.22	24.10	33.96	97.29
eraser	95.68	94.01	86.27	94.55	97.11	92.39	99.80	51.21	52.48	98.90
fire_hood	91.90	87.78	80.23	91.84	95.52	90.10	99.64	49.68	53.64	97.69
mint	81.56	80.79	72.80	86.02	96.30	90.81	98.78	29.23	39.46	90.63
mounts	87.38	73.09	78.76	99.74	99.87	98.93	99.63	42.78	45.86	96.89
pcb	94.40	96.68	89.36	95.34	97.90	92.35	99.61	62.03	60.32	96.94
phone_battery	93.82	91.71	83.86	97.98	99.14	96.43	99.63	57.13	57.12	97.59
plastic_nut	92.86	87.81	80.77	98.03	98.99	95.24	99.77	45.77	46.43	98.64
plastic_plug	91.52	88.22	79.60	96.63	98.50	94.05	99.45	40.55	44.67	97.58
porcelain_doll	87.85	78.25	72.43	97.90	99.11	97.15	99.12	31.07	37.81	96.36
regulator	92.83	87.42	80.85	98.14	99.11	95.25	99.55	45.39	49.55	97.71
rolled_strip_base	99.46	99.73	98.09	99.61	99.84	99.22	99.83	55.04	59.12	99.24
sim_card_set	96.62	97.16	90.52	99.20	99.63	98.05	99.51	58.97	57.73	96.91
switch	97.75	97.98	93.48	99.50	99.81	98.44	99.39	70.12	68.72	98.04
tape	97.20	95.87	89.00	99.83	99.91	99.43	99.77	54.18	57.51	99.07
terminalblock	98.77	99.07	95.44	98.81	99.57	98.17	99.91	58.62	58.46	99.43
toothbrush	88.45	89.36	83.45	99.02	99.36	96.86	97.30	34.80	41.93	91.60
toy	92.95	95.06	87.32	98.42	99.17	96.30	98.78	32.06	35.51	97.00
toy_brick	89.42	87.80	79.35	89.40	94.58	87.86	98.89	44.36	49.73	93.22
transistor1	98.47	98.86	94.55	99.76	99.88	98.81	99.51	52.81	53.28	97.87
usb	94.35	93.55	86.00	95.95	97.97	93.13	99.66	47.34	50.53	98.61
usb_adaptor	85.38	77.66	74.02	95.12	97.30	93.75	99.53	30.92	37.01	97.02
u_block	94.73	91.66	83.35	99.29	99.62	97.82	99.66	53.35	56.13	98.26
vcpill	92.93	91.24	83.68	97.35	98.70	93.55	99.39	70.25	69.34	96.12
wooden_beads	92.05	91.47	82.61	93.57	97.69	91.57	99.47	52.10	55.67	96.73
woodstick	91.37	83.54	75.92	87.89	93.59	87.39	99.43	57.23	59.39	95.90
zipper	99.21	99.58	97.09	99.99	100.00	99.70	99.22	64.32	65.08	97.42
Mean	**93.11**	**90.86**	**84.80**	**96.44**	**98.28**	**94.99**	**99.39**	**48.32**	**51.51**	**96.97**

Table A12: Per-category results of Meganomaly-B on MANTA-Tiny. All values are percentages (%).

Type	Category	I-AUROC	I-AP	I-F1	O-AUROC	O-AP	O-F1	P-AUROC	P-AP	P-F1	P-AUPRO
agriculture	maize	80.87	57.99	57.97	83.89	73.91	70.42	89.70	30.01	37.07	70.53
	paddy	89.68	79.36	74.90	93.76	90.80	81.13	78.38	18.92	22.07	72.02
	soybean	94.10	83.67	78.20	94.33	88.15	82.41	90.12	43.73	48.68	72.42
	wheat	93.04	84.74	78.41	93.68	90.90	80.98	96.05	46.95	48.23	80.57
electronics	block_inductor	93.04	90.01	84.16	94.41	92.91	85.71	98.92	65.44	63.59	93.15
	copper_standoff	98.71	97.92	95.95	99.39	99.02	97.14	99.00	68.89	67.05	94.89
	flat_nut	96.67	93.29	86.04	96.94	94.83	86.05	98.95	65.08	62.25	95.77
	led	99.10	97.31	91.14	99.60	99.36	97.62	99.33	46.93	54.50	97.40
	led_pad	99.53	98.25	96.68	99.57	98.92	97.56	99.12	61.45	62.74	96.05
	long_button	98.59	95.56	91.98	98.55	96.05	93.67	98.62	45.22	49.08	94.23
	power_inductor	97.95	93.50	88.02	98.17	96.97	89.33	98.45	54.08	57.83	92.26
	short_button	96.66	92.74	85.84	97.41	95.88	88.66	99.08	63.33	64.23	97.01
	thin_resistor	98.81	97.66	93.02	99.83	99.68	96.84	98.52	53.24	58.67	94.68
	type_c	98.79	95.40	93.47	99.81	99.58	98.36	98.83	41.41	46.04	94.71
	wafer_resistor	97.02	95.68	93.04	97.73	97.06	94.62	99.27	70.11	63.91	95.84
groceries	coffee_beans	72.39	55.63	56.27	77.79	64.34	66.95	83.78	32.37	38.61	63.70
	goji_berries	86.80	82.23	73.74	92.28	90.29	81.14	93.83	57.98	57.91	80.08
	pistachios	78.91	59.23	57.75	82.84	73.19	66.67	80.80	17.21	24.10	66.41
mechanics	button	93.90	82.03	75.64	89.53	84.79	77.58	99.48	37.62	47.95	95.92
	gear	96.67	86.92	85.13	98.55	94.21	94.41	98.90	46.48	50.77	94.90
	nut	94.98	88.24	79.70	91.78	88.08	78.26	99.15	37.11	47.09	96.99
	nut_cap	89.43	73.40	70.42	91.87	85.89	81.16	98.53	35.21	42.01	93.92
	red_washer	97.83	96.41	91.80	97.62	96.46	90.78	98.85	32.53	42.43	96.42
	round_button_cap	98.55	95.82	87.59	99.07	98.17	93.49	99.41	44.76	51.90	97.31
	screw	95.98	90.22	83.25	98.16	97.86	94.29	98.34	52.15	57.46	93.96
	square_button_cap	98.06	94.17	87.97	99.39	98.81	95.00	99.31	60.92	61.36	96.47
	terminal	98.24	94.45	89.24	98.73	97.53	93.47	99.43	61.85	61.64	97.62
	wire_cap	96.11	87.35	82.06	97.21	93.39	92.00	98.73	34.69	42.54	95.81
	yellow_green_washer	94.33	90.24	81.46	96.60	94.58	85.91	95.62	27.13	40.39	93.00
medicine	capsule	99.53	99.02	96.90	99.54	99.35	97.49	95.46	75.99	71.62	88.97
	coated_tablet	99.09	97.36	91.76	99.21	98.44	93.05	99.82	87.76	82.20	98.50

Continued on next page

Table A12: Per-category results of Meganomaly-B on MANTA (continued).

Type	Category	I-AUROC	I-AP	I-F1	O-AUROC	O-AP	O-F1	P-AUROC	P-AP	P-F1	P-AUPRO
	embossed_tablet	98.32	93.11	89.24	98.97	98.36	94.31	98.90	53.44	57.03	96.65
	lettered_tablet	96.94	86.67	85.50	98.76	97.58	93.33	99.22	56.34	57.97	97.26
	oblong_tablet	95.77	83.81	83.50	96.12	94.46	86.52	98.42	43.06	48.91	94.21
	pink_tablet	97.59	95.11	90.03	99.01	98.56	95.56	99.46	68.20	67.22	96.80
	red_tablet	74.04	56.94	55.90	81.40	72.86	66.05	79.82	35.37	46.21	51.53
	white_tablet	98.38	93.85	90.30	99.22	98.90	96.30	98.39	50.67	52.67	96.44
	yellow_tablet	99.23	97.53	93.60	99.86	99.75	99.15	99.50	67.59	65.69	98.01
Mean		**94.31**	**87.71**	**83.36**	**95.54**	**92.89**	**88.25**	**96.20**	**49.77**	**53.20**	**90.06**

Table A13: Per-category results of Meganomaly-B on MVTec-AD. All values are percentages (%).

Category	I-AUROC	I-AP	I-F1	P-AUROC	P-AP	P-F1	P-AUPRO
carpet	99.96	99.99	99.44	99.08	66.72	67.49	97.15
grid	99.92	99.97	99.13	99.50	62.15	63.24	97.59
leather	100.00	100.00	100.00	99.10	45.23	47.28	97.89
tile	100.00	100.00	100.00	95.09	65.31	63.67	83.30
wood	99.91	99.97	99.17	96.30	57.29	57.65	92.65
bottle	100.00	100.00	100.00	98.83	85.46	81.14	96.09
cable	99.74	99.83	98.91	98.51	77.78	71.70	93.61
capsule	99.24	99.83	99.09	98.89	63.87	59.17	98.02
hazelnut	100.00	100.00	100.00	99.41	80.86	76.79	96.19
metal_nut	100.00	100.00	100.00	97.34	78.02	85.85	94.32
pill	99.75	99.96	99.29	98.35	71.66	68.29	97.81
screw	99.71	99.90	98.35	99.73	64.88	61.90	98.88
toothbrush	100.00	100.00	100.00	98.86	53.49	61.80	95.39
transistor	100.00	100.00	100.00	97.69	78.04	71.24	92.99
zipper	100.00	100.00	100.00	99.02	74.50	70.99	96.93
Mean	**99.88**	**99.96**	**99.56**	**98.38**	**68.35**	**67.21**	**95.25**

Table A14: Per-category results of Meganomaly-B on VisA. All values are percentages (%).

Category	I-AUROC	I-AP	I-F1	P-AUROC	P-AP	P-F1	P-AUPRO
candle	99.34	99.35	96.52	99.46	47.36	50.52	96.33
capsules	99.38	99.61	98.00	99.64	68.00	66.30	98.77
cashew	98.66	99.44	96.94	99.40	75.89	68.87	97.75
chewinggum	99.88	99.94	98.99	99.17	59.36	62.90	91.41
fryum	99.46	99.74	97.98	96.81	49.54	53.53	93.42
macaroni1	99.09	99.10	95.61	99.65	37.26	42.81	97.23
macaroni2	98.30	98.30	93.81	99.76	27.74	37.84	98.79
pcb1	99.15	99.04	97.00	99.64	83.26	76.89	96.28
pcb2	98.63	98.30	96.45	99.12	25.79	38.56	93.48
pcb3	99.35	99.39	97.03	99.10	33.70	37.67	94.09
pcb4	99.90	99.90	98.49	98.77	57.65	54.61	93.91
pipe_fryum	99.88	99.94	99.50	99.36	65.15	66.82	96.74
Mean	**99.25**	**99.34**	**97.19**	**99.16**	**52.56**	**54.78**	**95.68**

Table A15: Per-category results of Meganomaly-B on Uni-Medical. All values are percentages (%).

Category	I-AUROC	I-AP	I-F1	P-AUROC	P-AP	P-F1	P-AUPRO
Brain MRI	95.19	98.95	94.92	98.77	77.65	72.01	89.08
Liver CT	76.27	71.70	68.99	98.17	26.10	31.13	95.57
Retina OCT	92.63	90.71	84.92	96.57	64.99	61.75	86.53
Mean	**88.03**	**87.12**	**82.94**	**97.84**	**56.25**	**54.96**	**90.39**

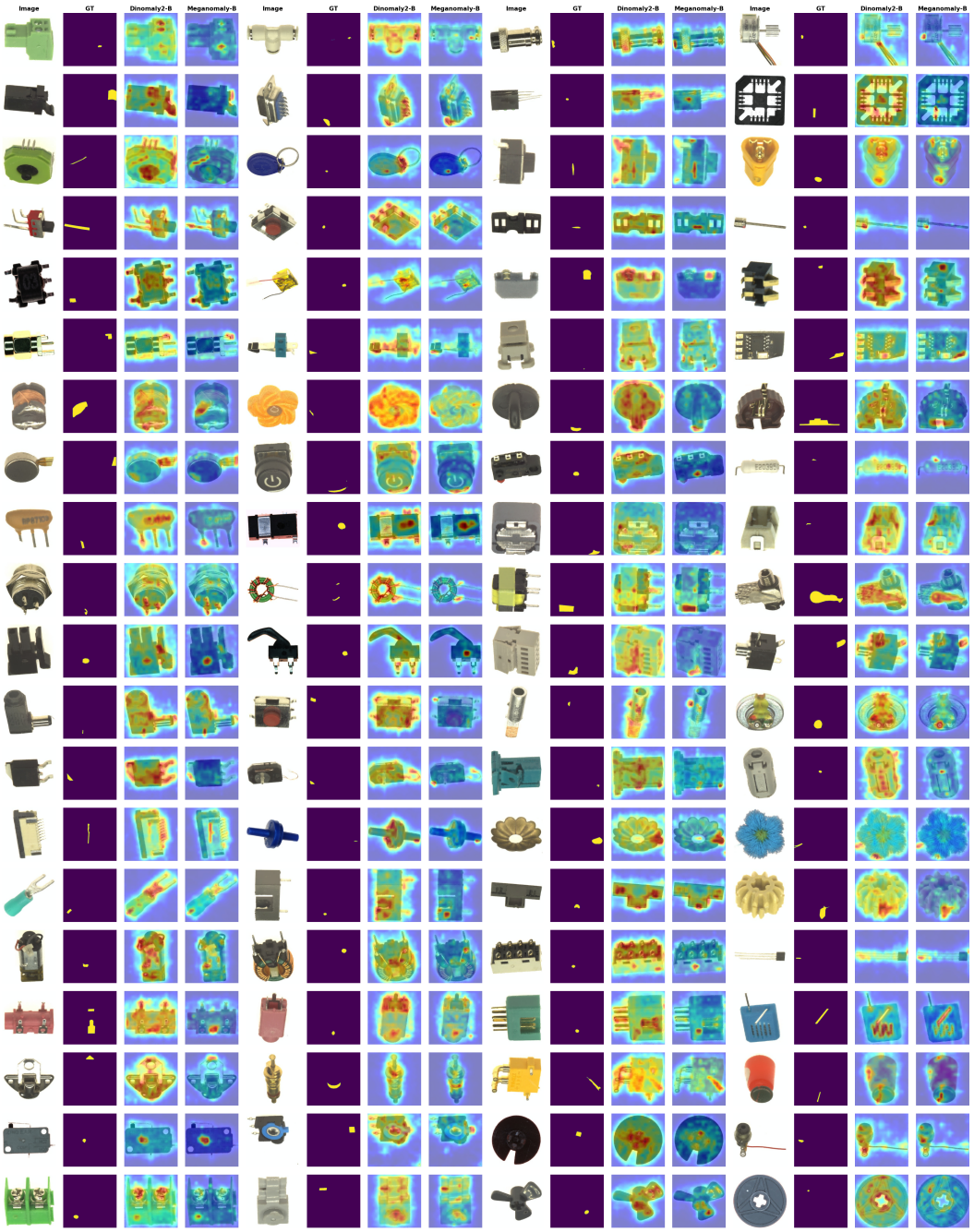


Figure A2: Visualization results on Real-IAD Variety, comparing Dinomaly2-B and Meganomaly-B.



Figure A3: Visualization results on Real-IAD Variety (continued).